Journal of Infrastructure Intelligence and Resilience 2 (2023) 100041

Contents lists available at ScienceDirect

Journal of Infrastructure Intelligence and Resilience

journal homepage: www.journals.elsevier.com/journal-of-infrastructure-intelligence-and-resilience

Structural displacement sensing techniques for civil infrastructure: A review

Zhanxiong Ma, Jaemook Choi, Hoon Sohn *

Department of Civil and Environmental Engineering, Korea Advanced Institute of Science and Technology, Daejeon, 34141, South Korea

ARTICLE INFO

Keywords:
Structural displacement sensing
Civil infrastructure
Single-mode sensor
Multi-mode sensor fusion
Long-term continuous monitoring

ABSTRACT

It is important to assess, monitor, and control civil infrastructure displacements, and extensive work has been done to develop structural displacement sensing techniques. This paper presents a comprehensive review of structural displacement sensing techniques, with particular focus on those for civil infrastructures. The working principles of structural displacement sensing techniques using thirteen different sensors are first reviewed, and the advantages and disadvantages of each sensor are briefly discussed. The disadvantages of single-mode sensor-based structural displacement estimation have been partially addressed by the use of multi-mode sensors. Thus, the studies on multi-mode sensor-based structural displacement estimation are reviewed. After that, field applications of these techniques to building structures, bridge structures, and other structures are briefly reviewed. The remaining challenges for the real application of these techniques are summarized, and future research directions are provided.

1. Introduction

In the field of civil engineering, structural failures can lead to catastrophic results. Thus, it is important to continuously monitor the health of a structure to prevent such failures. Structural health monitoring (SHM) aims to monitor, analyze, and identify various types of loads and structural responses of a target structure during its service life, thus enabling the assessment of the structure's performance and safety status. The displacement response plays a vital role in structural health monitoring because it assists in understanding the global behavior of a structure and evaluating its structural safety. It can be used in structural control and in disaster prevention and mitigation. The displacement has been directly used as a safety index in structural design codes in many countries such as the USA (AASHTO, 2017), South Korea (MLTM. Korea, 2010), China (MOHURD., 2020), and the EU (CEN. Eurocode 1, 2003). In addition, the displacement response has been used for bridge loading tests (Lee et al., 2006; Vicente et al., 2015; Dong et al., 2020; Sun et al., 2021; Hester et al., 2017), structural damage detection (Feng and Feng, 2016), modal identification (Feng and Feng, 2017; Kim et al., 2013; Bhowmick and Nagarajaiah, 2020; Jiao et al., 2021), and finite element model updating (Feng and Feng, 2015; Civera et al., 2020). Therefore, it is essential to monitor the structural displacement response.

Many factors should be considered when estimating the structural displacement. The most important of these is the performance of the measurement method, which should have a sufficient frequency range and measurement accuracy, as well as the ability to measure the displacements in multiple directions and at multiple points. The second thing that should be considered is the sensor installation location. A sensor can be installed at displacement-measurement locations for contact-type displacement measurement or installed at other locations for noncontact displacement measurement. Note that the sensor installation location should be selected based on the purpose of the displacement measurement, i.e., whether it is used in a short-term survey or long-term continuous monitoring. In addition, the data transmission and power supply, and the robustness to time-varying operational and environmental conditions such as extreme weather conditions, occlusion, or illumination variation should be considered, especially for long-term continuous displacement monitoring.

Many techniques have been developed for structural displacement measurement, and the sensors used in these techniques (Fig. 1) can be divided into the (1) contact and (2) noncontact types, depending on whether access to the displacement measurement point is required or not. Linear variable differential transformers (LVDTs) (Nassif et al., 2005; Santhosh and Roy, 2017), accelerometers (Lee et al., 2010; Gomez et al., 2018; Park et al., 2013a; Gindy et al., 2008; Wang et al., 2011), inclinometers (Hou et al., 2005; Zhang et al., 2017a), strain sensors (Shin et al., 2012; Zhang et al., 2017b, 2018a, 2021; Wang et al., 2014; Kim and Cho, 2004; Shen et al., 2010; Xia et al., 2014; Sigurdardottir et al., 2017; Chen et al., 2017a), connecting pipe systems (Liu et al., 2015; Zhou et al., 2021), optical fiber sensors (Lee et al., 2022a; Bonopera et al., 2019;

* Corresponding author.
E-mail addresses: mazhanxiong@kaist.ac.kr, cjmook@kaist.ac.kr, hoonsohn@kaist.ac.kr (H. Sohn).

https://doi.org/10.1016/j.iintel.2023.100041
Received 21 January 2023; Received in revised form 14 March 2023; Accepted 12 April 2023
Available online xxxx

Fig. 1. Sensors used for structural displacement measurement.

Rodrigues et al., 2011; Chan et al., 2009), and global navigation satellite systems (GNSS) (Xiong et al., 2022; Niu et al., 2021; Tamura et al., 2002; Nakamura, 2000) are typical contact-type sensors. An LVDT can measure displacement with high accuracy, but the requirement of an additional scaffold for the installation makes it less attractive in real applications. Accelerometers are the most widely used type for displacement estimation, but acceleration-based displacement either suffers from a large, low-frequency drift or loses important low-frequency structural displacement information. Although both strain sensors and inclinometers can estimate both low- and high-frequency displacements, multiple sensors are required even for displacement estimation at a single point. A connecting pipe system can simultaneously estimate the structural displacements at multiple locations, but can only estimate vertical displacements. Optical fiber sensors can only measure the relative displacement between two points of a target structure. Currently, a GNSS is commonly adopted in the SHM systems of many large-scale bridges and building structures for long-term displacement monitoring, but it typically has a low sampling rate of up to 20 Hz and low accuracy of approximately 7–10 mm. Moreover, it cannot work in a GNSS-denied environment.

All the above-mentioned sensors must be placed at a displacement measurement point of a target structure, but access to such displacement measurement points may not be available in some applications. Efforts have been made to develop various noncontact displacement estimation techniques using vision cameras (Feng et al., 2015; Luo and Feng, 2018; Dong et al., 2019; Yoon et al., 2018; Shang and Shen, 2018; Chen et al., 2017b; Khuc and Catbas, 2017a; Yu and Zhang, 2020; Luan et al., 2021; Xu et al., 2021; Zhu et al., 2021; Jeong and Jo, 2022; Lee and Shinozuka, 2006), radars (Zhang et al., 2020; Gentile and Bernardini, 2008, 2010; Owerko and Kuras, 2019; Guan et al., 2017, 2018; Rodrigues et al., 2021; Guo et al., 2021), laser Doppler vibrometers (LDV) (Reu et al., 2017; Toyoshima et al., 1994), laser triangulation sensors (LTS) (Zhuojiang et al., 2021), light detection and ranging (LiDAR) (Blais, 2004; Lee et al., 2019; Lee and Kim, 2022; Park et al., 2007), level (Corsetti et al., 2018; Zhou et al., 2020a), and total stations (TS) (Zhou et al., 2020a; Yu et al., 2017; Psimoulis and Stiros, 2007; Stiros and Psimoulis, 2012). However, vision-based techniques have a high computational cost and their accuracies are highly sensitive to illumination conditions. An LDV requires a reflector installed at the displacement estimation point to ensure stable signal reflection, and laser beams with high intensity are needed for long-distance measurements, which pose a health risk to humans. An LTS also requires a reflector and is only suitable for short-distance measurement. LiDAR is advantageous for full-field structural displacement estimation, but it has limited accuracy. Radar requires the manual identification of the position of the radar-detected target on the target structure, and manual estimation of the conversion factor is required to convert the line-of-sight (LOS) displacement into the structural displacement in the actual direction of vibration. In addition, large structural displacement measurements may suffer from a phase-wrapping issue, especially when using millimeter-wave radars, resulting in inaccurate displacement estimation. Level and TS are not suitable for high-sampling-rate or long-term displacement monitoring and are often used as reference sensors to evaluate the displacement estimation performances of other sensors.

Each of these structural displacement estimation techniques has its advantages and disadvantages. Thus, another trend in structural displacement estimation is to combine data from different sensors for improved displacement estimation. Most commonly, an accelerometer is combined with other sensors such as strain sensors (Zhu et al., 2020; Zhou et al., 2022), vision cameras (Park et al., 2018; Chang and Xiao, 2010; Xu et al., 2019), or a GNSS (Xu et al., 2017; Koo et al., 2017). A general framework for estimating the displacement by combining an accelerometer with other sensors is given in Fig. 2. Acceleration and initial displacement measurements from other sensors are combined using either a Kalman or finite impulse response (FIR) filter to obtain the final displacement with improved accuracy and/or an increased sampling rate. In addition, sensor fusion has been explored, including applications that combined strain sensors and inclinometers (Sun et al., 2020), an LDV and LiDAR (Kim and Sohn, 2017; Kim et al., 2016a), a vision camera and an LDV (Nasimi and Moreu, 2021a, 2021b), and a vision camera and LiDAR (Lee et al., 2022b).

This paper aims to present a comprehensive review of structural displacement estimation techniques, with the main focus on civil infrastructures. The remaining challenges for the real applications of these techniques are discussed, along with the future outlook. Although reviews have previously been performed on structural displacement measurement methods, they either focused on a particular class of displacement measurement techniques (e.g., GNSS-based techniques (Wang et al., 2021; Shen et al., 2019; Yu et al., 2020), vision-based techniques (Feng and Feng, 2018; Xu and Brownjohn, 2018; Zhuang et al., 2022), or radar-based techniques (Monserrat et al., 2014)), or they focused on the general area of SHM (Wu and Jahanshahi, 2020; Dong and Catbas, 2021; Spencer et al., 2019), while only briefly reviewing structural displacement measurement as an important sub-topic. The remainder of this paper is organized as follows. Structural displacement estimation techniques using single-mode sensors and multi-mode sensors are reviewed in sections 2 and 3, respectively. Then, domain-specific applications are reviewed in section 4, followed by a discussion of considerations for structural displacement estimation and the remaining challenges. Finally, section 5 concludes the paper with a summary and future outlook.

2. Structural displacement measurement techniques using single-mode sensor

Depending on whether access to the displacement measurement point is required or not, the techniques can be divided into two types: (1) contact and (2) noncontact types. Table 1 compares all the sensors for structural displacement estimation discussed in this section in terms of (1) displacement-measurement accuracy, (2) sampling rate, (3) requirement of a stationary installation location, (4) displacement-measurement direction, (5) ability to perform multi-point displacement estimation, (6) potential for long-term displacement monitoring, and (7) computation

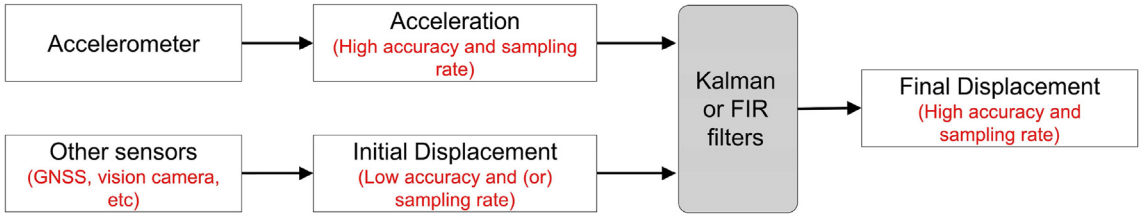

Fig. 2. General framework of structural displacement estimation fusing accelerometer with other sensors.

efficiency. This section discusses more details, including the working principles, advantages, and disadvantages of these sensors.

2.1. Contact-type measurement

2.1.1. LVDT

An LVDT is commonly used for displacement measurement in the field of civil engineering (Nassif et al., 2005; Santhosh and Roy, 2017). It consists of a cylindrical form with a movable soft iron core, as shown in Fig. 3. A primary winding (P) is connected to an AC voltage source, and two secondary windings (S_1 and S_2) are wound on the cylindrical form. Then, AC voltages are induced in S_1 and S_2 (E_{S1} and E_{S2}, respectively) by the alternating magnetic field produced by the AC voltage in P. For bridge displacement measurement, the LDVT is fixed on a stationary scaffold or solid support structure, and the movable soft iron core is in direct contact with the target structure. The core movement (i.e., bridge displacement) causes variations in E_{S1} and E_{S2}, where the difference between them ($E_o = E_{S1} - E_{S2}$) is proportional to the bridge displacement (Santhosh and Roy, 2012). Therefore, the bridge displacement can be obtained by measuring E_o. An LVDT is one of the most commonly used devices for measuring displacement in the field of civil engineering (Nassif et al., 2005; Santhosh and Roy, 2017). Although LVDTs have good measurement accuracy, their installation is cumbersome and difficult, which limits their applications in the long-term monitoring of large-scale structures. In addition, the performance of an LVDT also degrades in practical applications because of unexpected scaffold vibration.

2.1.2. Accelerometer

Acceleration sensors are commonly used for structural displacement estimation because of their easy installation and low computational cost. By integrating acceleration measurements twice, the displacement can easily be estimated based on the physical relationship between the displacement and acceleration. Nevertheless, unknown initial conditions (i.e., the initial displacement and velocity) and acceleration measurement noises lead to a large, low-frequency drift in the estimated displacement. Such a drift can be effectively removed with a high-pass filter (Lee et al., 2010; Gomez et al., 2018; Park et al., 2013a), but the filter also suppresses important low-frequency structural displacements because of the difficulties in distinguishing the actual structural response in the low-frequency band from the noise. Many techniques such as state-space (Gindy et al., 2008) and iteration-based techniques (Wang et al., 2011) have also been developed to recover the low-frequency structural displacement, but such low-frequency displacements still cannot be estimated stably.

2.1.3. Inclinometer

Attempts have also been made to estimate structural displacement using inclinometers (Hou et al., 2005). Assuming that rotations are measured at multiple points using inclinometers ($x = x_i, i = 1, \cdots, V$), the rotation distribution at each time step can be fitted using a W-order polynomial function ($W \leq V - 1$).

$$\begin{bmatrix} \theta(x_1) \\ \vdots \\ \theta(x_V) \end{bmatrix} = \begin{bmatrix} 1 & \cdots & x_1^W \\ \vdots & \ddots & \vdots \\ 1 & \cdots & x_V^P \end{bmatrix} \begin{bmatrix} G_0 \\ \vdots \\ G_W \end{bmatrix} \tag{1}$$

The W unknown coefficients ($G_0, \cdots, G_W$) can be estimated using a least square estimation algorithm. According to the Euler–Bernoulli beam theory, the rotation–displacement relationship can be expressed as follows:

$$\theta(x) = \frac{du(x)}{dx} \tag{2}$$

Then, the displacement distribution can be integrated from the rotation distribution as follows:

$$u(x) = \int_0^L \theta(x)dx = G_0 x + G_1 x^2 + \cdots + G_P x^{P+1} \tag{3}$$

Note that the integration constant in Equation (3) equals zero because of the boundary condition of $u(0) = 0$. With the help of the finite element model of a target structure, a similar algorithm was proposed by Zhang et al. (2017a), which considered structural damages. Although the full-field structural displacement can be estimated, multiple inclinometers should be installed along the target structure. In addition, high-accuracy rotation measurement is still challenging, especially in the low-frequency band.

2.1.4. Strain sensor

Strain sensors are extensively used for structural displacement estimation, along with a mode superposition algorithm (Shin et al., 2012; Zhang et al., 2018a). Assuming that strains are measured at N points ($\varepsilon_k(x_1), \cdots, \varepsilon_k(x_N)$) at the kth time step, the vertical displacement ($u_k(x_d)$) of a beam at any desired point ($x = x_d$) can be estimated from the strain measurements according to the Euler–Bernoulli beam theory:

$$u_k(x_d) = \frac{1}{y_c} \boldsymbol{\Psi}(x_d) \left[\boldsymbol{\Phi}(x)^{\mathrm{T}} \boldsymbol{\Phi}(x) \right]^{-1} \boldsymbol{\Phi}(x)^{\mathrm{T}} \boldsymbol{\varepsilon}_k(x) \tag{4}$$

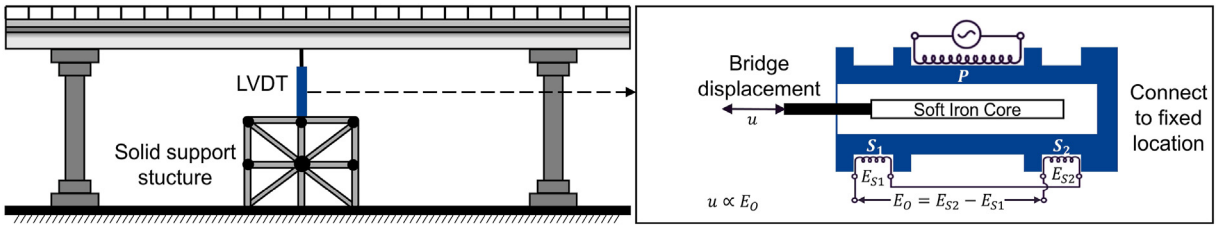

Fig. 3. Overview of LVDT-based bridge displacement measurement.

$$\boldsymbol{\Psi}(x_d)=[\varphi_1(x_d)\quad\cdots\quad\varphi_N(x_d)];\ \boldsymbol{\Phi}(x)=\begin{bmatrix}\varphi_1(x_1)&\cdots&\varphi_N(x_1)\\ \vdots&\ddots&\vdots\\ \varphi_1(x_N)&\cdots&\varphi_N(x_N)\end{bmatrix};\quad \boldsymbol{\varepsilon}_k(x)=\begin{bmatrix}\varepsilon_k(x_1)\\ \vdots\\ \varepsilon_k(x_N)\end{bmatrix} \tag{5}$$

vwhere $\varphi_j(x)$ and $\varphi_j(x)$ denote the jth displacement and strain mode shapes, respectively. y_c denotes the vertical distance from the strain measurement point to the neutral axis. However, the mode superposition algorithm requires prior knowledge of the mode shapes and neutral axis location of a target structure, which may not be readily available for many applications. Efforts have been made to estimate strain-mode shapes directly from strain measurements and estimate displacement-mode shapes using double integration (Wang et al., 2014; Zhang et al., 2021). However, the accurate estimation of strain-mode shapes is difficult in practice considering the large noise level in field strain measurements.

The need for mode shapes has been eliminated using a curve-fitting algorithm (Kim and Cho, 2004), conjugate-beam algorithm (Shen et al., 2010), and virtual-work algorithm (Xia et al., 2014). The working principle of the curve-fitting algorithm is similar to that of inclinometer-based displacement estimation. The strain distribution is first fitted using multiple strain measurements, and then the displacement distribution is estimated using double integration. However, the algorithm still requires the neutral axis location, and dense strain gauges are needed to reduce the integration-induced error in the estimated displacement (Sigurdardottir et al., 2017). The conjugate-beam algorithm can estimate the displacement induced by bending, support settlements, temperature variations (Shen et al., 2010), and even shear forces (Zhang et al., 2017b; Chen et al., 2017a), but the neutral axis location is still required and long-gauge FBG strain sensors should be used, which are rather expensive. Although the virtual-work algorithm does not require a neutral axis location, it only works for cantilever-type structures with uniform sections.

2.1.5. Connecting pipe system

A connecting pipe system was proposed to measure the vertical displacements of a bridge at multiple points (Liu et al., 2015; Zhou et al., 2021) based on the working principle summarized in Fig. 4. After measuring the pressures at a reference point (P_R) and displacement measurement point (P_i), the vertical distance between the reference and measurement points (ΔH_i) can be obtained as follows:

$$\Delta H_i=\frac{P_i-P_R}{\rho g} \tag{6}$$

where ρ and g denote the water density and gravitational acceleration, respectively. Considering that the reference point is fixed, the variation of ΔH_i becomes the displacement at the ith location. Although connecting pipe systems can simultaneously estimate bridge displacements at multiple locations, they can only estimate vertical displacements.

2.1.6. Optical-fiber sensor

Fig. 5 shows the overall working principle of optical-fiber sensors (Ramakrishnan et al., 2016). A light source outputs light through an optical fiber into the modulation area. The displacement, temperature variation, etc. applied at the modulation area causes a change in the optical parameters of the optical signal, such as the intensity, phase, and spectrum. Then, a modulated light signal is generated and received by the light detector. Finally, the displacement, temperature variation, etc. can be estimated by demodulation. Optical-fiber sensors can be employed in several different ways for structural displacement estimation. Their use is similar to that of an LVDT. One side of the fiber is fixed on a stationary scaffold or solid support structure, and the other side is in direct contact with a target structure. The displacement of the structure will strain the fiber, which is monitored through optical interrogation of the Bragg wavelength. Optical fiber sensors have also been used for strain and inclination measurements. Thus, algorithms explained in sections 2.1.3 and 2.1.4 can be used to estimate the displacement based on the measured strain (Kim and Cho, 2004) or inclination (Chan et al., 2009). In addition, optical fiber sensors have been integrated with connecting pipe systems for long-term bridge displacement monitoring (Lee et al., 2022a; Bonopera et al., 2019; Rodrigues et al., 2011).

2.1.7. GNSS

A GNSS satellite sends an intermittent radio signal to the earth, which contains the exact time the signal was sent (T_i) and the coordinates of the satellite ((X_i, Y_i, Z_i)). Assuming that M satellites are available and the transmitted signals are simultaneously received by a GNSS receiver installed at a target structure at time T_G, the distances between the GNSS receiver and satellites ($D_i, i=1,\cdots,M$) can be expressed as follows:

$$\begin{cases} D_1=\sqrt{(X_G-X_1)^2+(Y_G-Y_1)^2+(Z_G-Z_1)^2}=c(T_G-T_1)\\ \vdots\\ D_M=\sqrt{(X_G-X_M)^2+(Y_G-Y_M)^2+(Z_G-Z_M)^2}=c(T_G-T_M)\end{cases} \tag{7}$$

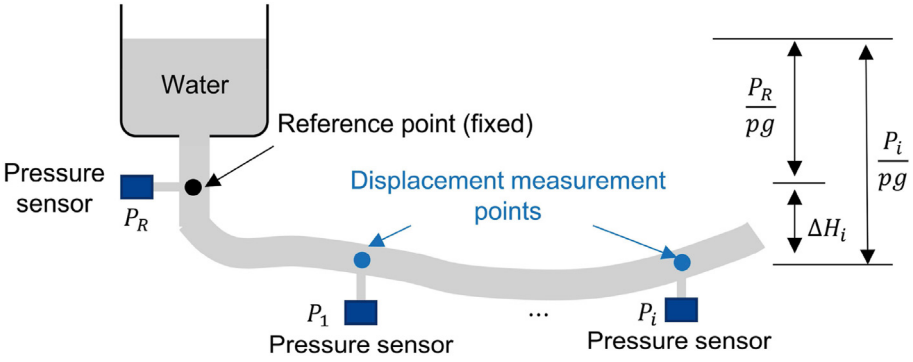

Fig. 4. Overview of bridge displacement estimation using a connecting pipe system.

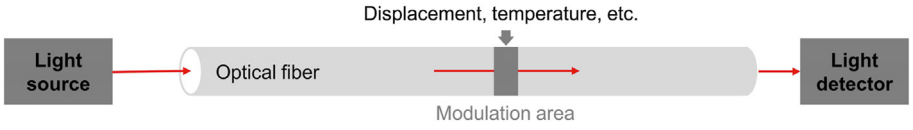

Fig. 5. Overall working principle of optical fiber sensor.

where (X_G, Y_G, Z_G) denote the coordinates of the GNSS receiver, and c denotes the speed of light. With $M \geq 4$, the values of (X_G, Y_G, Z_G) and T_G are estimated from Equation (7). The variations of (X_G, Y_G, Z_G) become the three-dimensional (3D) structural displacements (Kaplan and Hegarty, 2017).

GNSS-based positioning originally has a meter-level accuracy, which is insufficient for structural displacement estimation. The displacement-measurement performance can be enhanced using a real-time kinematic (RTK) technique by adopting two GNSS receivers. One receiver called a base is installed at a stationary location, and the other receiver called a rover is installed at a target structure. The rover measurement can be corrected by subtracting the base measurement from the rover measurement assuming that both the rover and base share a common environment and clock error (Hofmann-Wellenhof et al., 2012). An RTK-GNSS has been adopted to measure the displacements of buildings (Tamura et al., 2002) and suspension bridges (Nakamura, 2000), and various attempts have also been made to denoise GNSS-based displacements using various signal processing algorithms (Xiong et al., 2022; Niu et al., 2021). However, GNSS-based displacement measurement has limited accuracy of up to 5–8 mm and a limited sampling rate of up to 10 Hz. In addition, its performance is greatly degraded by GNSS satellite signal blockage or multi-pathing error. Moreover, it is not suitable for GNSS-denied environments such as underwater environments.

2.2. Noncontact measurement

2.2.1. Vision camera

Vision cameras have been widely employed for noncontact bridge displacement estimation. Fig. 6 shows an overview of vision-based structural displacement estimation. A vision camera is usually installed at a stationary location with its lens aimed at a natural or artificial target at the displacement estimation point (Fig. 6(a)). Then, the target movement is first estimated in pixel units from vision measurements using template-matching algorithms (Feng et al., 2015; Luo and Feng, 2018), optical-flow algorithms (Dong et al., 2019; Yoon et al., 2018), phase-based algorithms (Shang and Shen, 2018; Chen et al., 2017b), feature-matching algorithms (Khuc and Catbas, 2017a; Yu and Zhang, 2020), or deep-learning algorithms (Luan et al., 2021; Xu et al., 2021; Zhu et al., 2021; Jeong and Jo, 2022). Then, it is converted into the displacement in length units using a scale factor, which can be estimated by identifying the target dimensions in physical units in advance (Lee and Shinozuka, 2006) (Fig. 6(b)). In addition, attempts have also been made to reduce the displacement estimation errors induced by camera ego-motion (Ma et al., 2022a; Yu et al., 2022), environmental temperature variation (Zhou et al., 2020b), optical-turbulence (Luo et al., 2020), illumination variation (Yang et al., 2022), etc. However, the following limitations still exist. First, the manual measurement of the target dimensions for scale-factor estimation may be challenging under field conditions. Second, the high computational cost of these techniques hinders the real-time estimation of displacement at a high sampling rate. Third, securing a stationary location to install the vision camera can be difficult, especially for long-term continuous monitoring.

The need for a stationary camera installation location has been eliminated by installing a camera on a target structure (Yu and Zhang, 2020) or drone (Yoon et al., 2018; Weng et al., 2021). For the former, the structural displacement can be continuously estimated by tracking a stationary target in the area surrounding the target structure. Except for this, the displacement estimation procedure is identical to that using a fixed camera. For the latter, the relative displacement between the camera and target structure is first estimated using the procedure shown in Fig. 6(b). Then, the camera vibration (i.e., drone vibration) is estimated by tracking other stationary targets. However, the drone has a six-degree-of-freedom (6-DOF) vibration, which makes the accurate estimation of the vibration challenging. In addition, these techniques are only suitable for short-term structural displacement surveys.

2.2.2. Radar

Fig. 7 shows a flowchart of noncontact structural displacement estimation using a frequency-modulated continuous wave (FMCW) radar. At the kth time step, the radar transmits a frequency-modulated (FM) signal $(S_T(t))$ with a duration of T_c,

$$S_T(t) = e^{j\left(2\pi f_s t + \pi K t^2\right)} \ (k\Delta t \leq t \leq k\Delta t + T_c) \tag{8}$$

where f_s and K denote the starting frequency and frequency slope of the FM signal, respectively. The transmitted signal is reflected by multiple targets (Q) in the area surrounding the radar, and a mixed signal $(S_R(t))$ of these reflected signals is obtained,

$$S_R(t) = \sum_{m=1}^{Q} S_R^m(t) = \sum_{m=1}^{Q} \delta^m S_T(t - \Delta t^m) = \sum_{m=1}^{Q} \delta^m S_T(t - 2D^m / c) \tag{9}$$

where δ^m and Δt^m denote the attenuation factor and traveling time of the mth target, respectively. D^m denote the LOS distance from the radar to the mth target, and c denotes the speed of light. Next, an intermediate frequency (IF) signal is calculated as follows:

$$IF(t) = S_T(t) \times S_R^*(t) = \sum_{j=1}^{Q} \delta^m e^{j(\varphi^m + \omega^m t)}; \omega^m = \frac{4\pi K D^m}{c}; \ \varphi^m = \frac{4\pi f_s D^m}{c} \tag{10}$$

Note that both the frequency (ω^m) and phase (φ^m) of the IF signal include distance information (D^m). After that, the Fourier transform is applied to the IF signal, and peaks in the amplitude spectrum correspond

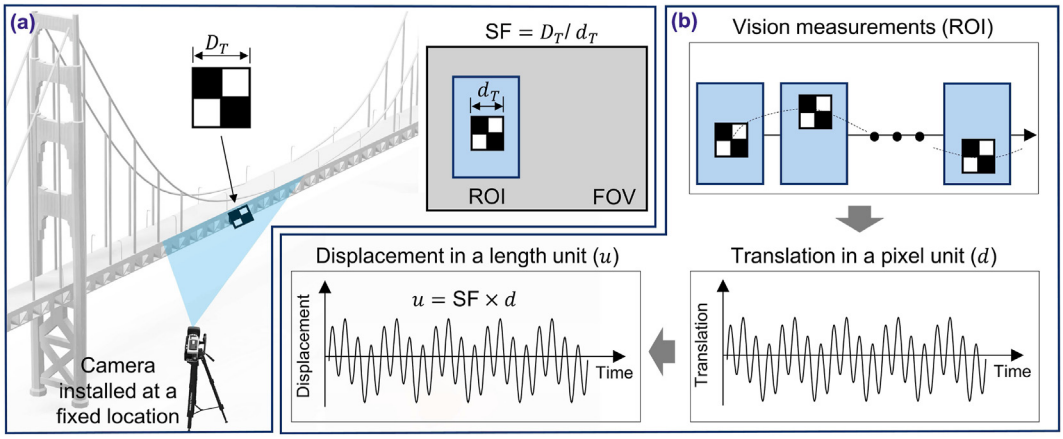

Fig. 6. Overview of structural displacement estimation using a camera installed at a fixed location: (a) sensor setup and (b) overall flowchart.

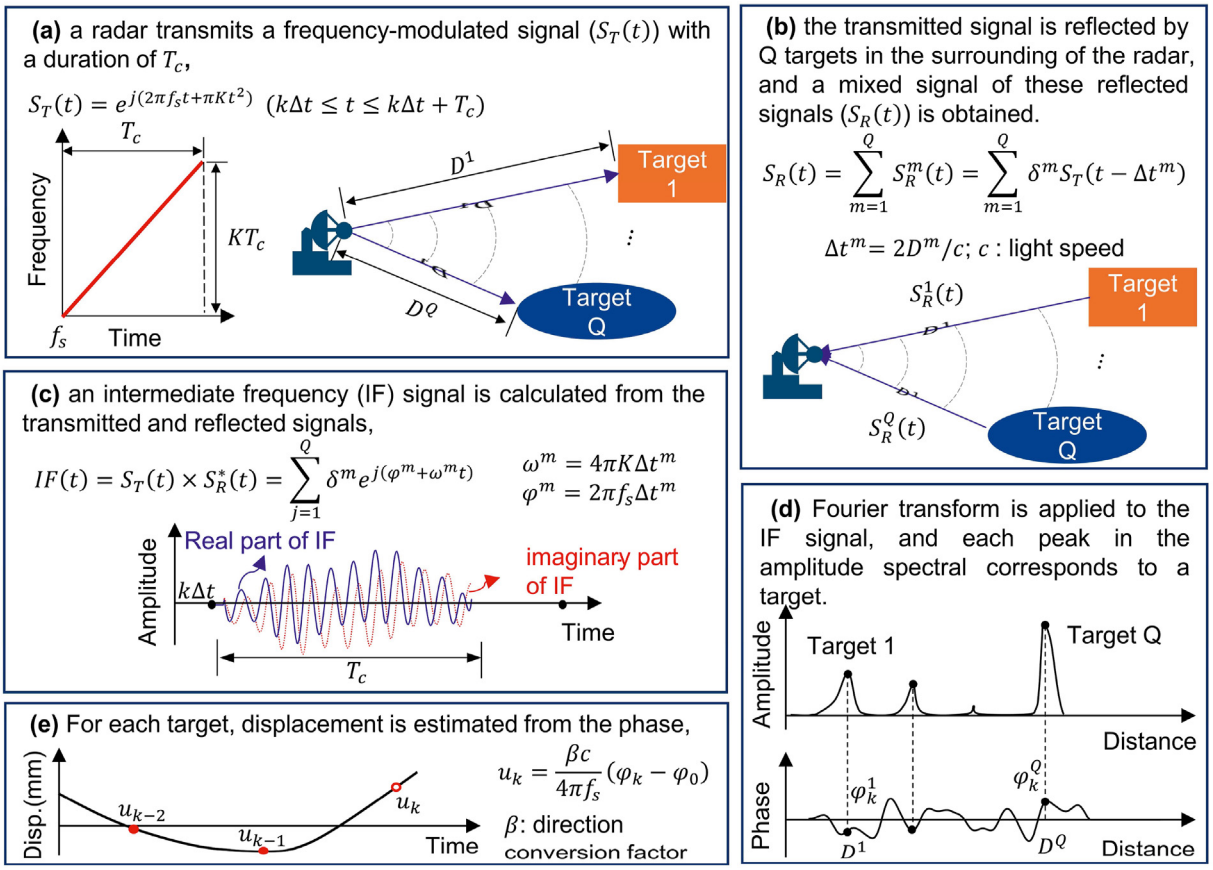

Fig. 7. Flowchart of FMCW radar-based structural displacement measurement.

to targets at different distances. Because the radar vibration is very small, the phase is commonly adopted to estimate the displacement of each target:

$$u_k^m = \beta^m \frac{c}{4\pi f_s}(\varphi_k^m - \varphi_0^m) \tag{11}$$

where φ_0^m and φ_k^m denote the initial and current phases extracted from the mth target, respectively. Note that the actual target vibration direction may differ from the LOS direction, and a direction conversion factor (β^m) is included in Equation (11).

Over the last two decades, extensive studies have been conducted on structural displacement estimation for bridges and building structures using microwave (Zhang et al., 2020; Gentile and Bernardini, 2008, 2010; Owerko and Kuras, 2019; Guan et al., 2017, 2018) or millimeter-wave radars (Rodrigues et al., 2021; Guo et al., 2021). In all these studies, a radar is installed at a stationary location, and the multi-point displacements of the target structure are estimated as shown in Fig. 8(a). However, to select a target near the desired displacement estimation point and then estimate the conversion factor (β^m) for the selected target, the locations of all the radar-detected targets on the target structure should be manually identified, which is cumbersome. In addition, when the structural displacement exceeds the radar wavelength, phase wrapping could be a major issue, especially for millimeter-wave radars. Moreover, securing a stationary installation location may not be possible, especially for long-term continuous displacement monitoring. A few attempts have been made to install a radar on a target structure (Guan et al., 2017, 2018), as shown in Fig. 8(b), to eliminate the need for a stationary installation location. However, they required the installation of an active transponder at a stationary location, which would be cumbersome in practice.

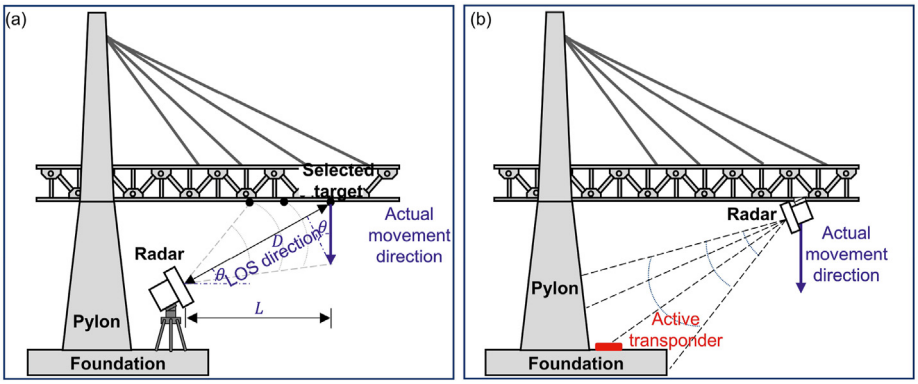

Fig. 8. Sensor setup for radar-based structural displacement estimation: (a) a fixed radar at a stationary location and (b) radar installed on a target structure.

2.2.3. Laser-based sensor

Laser-based sensors have also been adopted for noncontact structural displacement estimation. Although various laser-based sensors are available, they use three different laser ranging algorithms: (1) pulse-based algorithm, (2) phase-based algorithm, and (3) triangulation algorithm. Fig. 9 briefly shows the working principles of these three algorithms. The pulse-based algorithm uses a laser pulse, and the distance between the radar and target (D) is estimated from the laser return time (Fig. 9(a)). The phase-based algorithm uses a sinusoidal laser, and D is estimated from the phase shift between the transmitted and reflected lasers (Fig. 9(b)). The triangulation algorithm is quite different from the previous two algorithms. The transmitted laser is reflected by the target and detected by an image sensor. D can be estimated from the laser position in the image sensor (Fig. 9(c)). Note that all three algorithms estimate D, and its variation with respective to time becomes the target displacement.

The first type of laser-based sensor is the LDV (Reu et al., 2017; Toyoshima et al., 1994), which uses the phase-based algorithm. For displacement measurement, an LDV is installed on the fixed ground and focused on the target (i.e., the displacement estimation point). Although the displacement can be estimated with very high accuracy, the following limitations exist. First, to achieve a stable signal reflection, a reflector with a retroreflective film should be mounted at the displacement estimation point, and the laser beam should be perpendicular to the reflector surface. Second, because LDVs are fairly expensive, it may not be possible to widely utilize them for structural displacement monitoring. Third, laser beams with high intensity are needed for long-distance measurements, which pose a health risk to humans (Nassif et al., 2005). The second type of laser-based sensor is an LTS (Zhuojiang et al., 2021), which uses the triangulation algorithm. The sensor setup for an LTS is the same as that for an LDV. However, it only has sufficient accuracy when the distance between the LTS and target is short. Therefore, an LTS is mainly used in laboratory tests to measure ground-truth displacements. The last type of laser-based sensor is a LiDAR (Blais, 2004; Lee et al., 2019; Lee and Kim, 2022; Park et al., 2007), which uses either a pulse-based or phase-based algorithm. Using a galvanometer and rotating mechanical station, the LiDAR scans objects in three dimensions and generates their three-dimensional coordinates. Note that the LDV and LTS estimate single-point displacements in the LOS direction, but a LiDAR can estimate three-dimensional and full-field displacements. However, the displacement estimation performance of a LiDAR is much worse than those of an LDV and LTS. Currently, most LiDARs can only measure displacements with an accuracy of 2–3 cm, while LiDARs that can estimate displacements with millimeter-level accuracy are fairly expensive. Fig. 10 summarizes the advantages and disadvantages of these three different laser-based sensors.

2.2.4. Level

A level is a traditional instrument used for structural vertical-displacement measurement. Fig. 11(a) shows an overview of level-based structural vertical-displacement estimation. A level is installed at a stationary location and properly leveled to ensure that the optical axis of the telescope of the level is in a horizontal direction. A leveling rod is installed on a target structure, and a height value (H_R) can be obtained by focusing the telescope on the leveling rod. Finally, the variation of H_R becomes the vertical displacement of the target structure. In previous studies, levels have been adopted to measurement the displacements of bridges (Zhou et al., 2021; Yu and Zhang, 2020), dams (Corsetti et al., 2018), and underground tunnels (Zhou et al., 2020a), and these measured displacements were used as reference displacements to evaluate techniques developed using other sensors. Note that even though a high-accuracy displacement can be achieved using a level, the manual leveling and measurement requires well-trained workers, and inaccurate operation may lead to large displacement measurement errors. Moreover, it is not suitable for high-sampling-rate or long-term continuous displacement monitoring.

2.2.5. TS

A TS is another traditional instrument used for structural displacement estimation. Similar to a level, it measures the vertical displacement as the variation of a target height. Fig. 11(b) gives an overview of TS-based vertical displacement estimation. A TS installed at a stationary

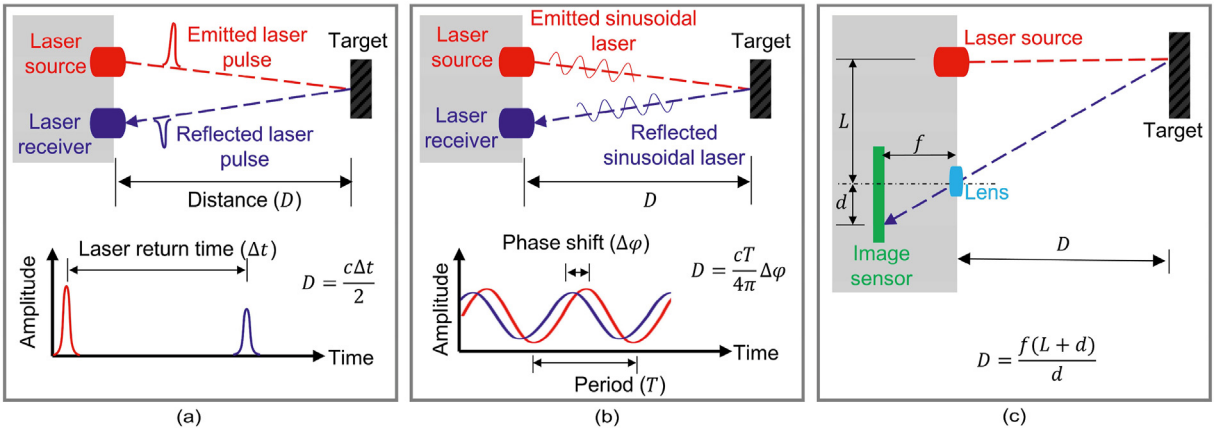

Fig. 9. Working principles of three different laser ranging algorithms: (a) pulse-based algorithm, (b) phase-based algorithm, and (c) triangulation algorithm.

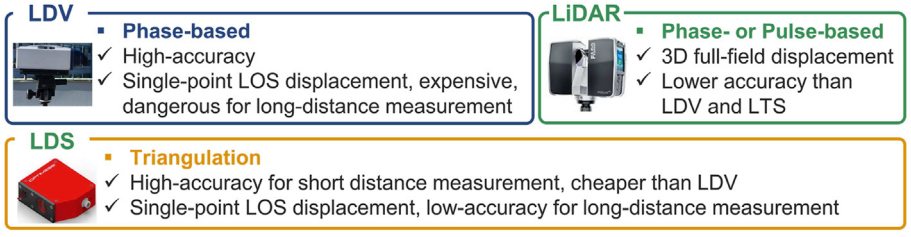

Fig. 10. Comparison of three different laser-based sensors (i.e., LDV, LTS, and LiDAR).

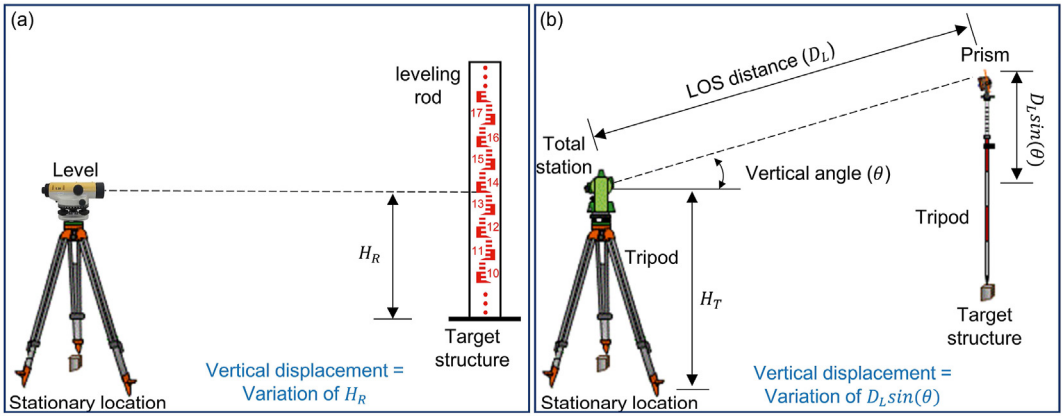

Fig. 11. Overview of (a) level-based and (b) TS-based vertical displacement estimation.

location emits a modulated wave, which is reflected by a prism installed at a target structure. Then, the LOS distance between the TS and target (D_L), and the angle of the sighting line relative to the horizontal axis (θ), are estimated by analyzing the emitted and reflected waves. The height of the prism can be estimated as ($H_T + D_L\ sin\ (\theta)$). Considering that the height of the tripod (H_T) is constant, the variance of $D_L\ sin\ (\theta)$ with respective to time becomes the vertical displacement of the target structure. Note that the basic principle of a TS is explained here for vertical-displacement estimation, but a TS can be easily extended to both horizontal- and vertical-displacement estimation by measuring the horizontal angle of the sighting line relative to a certain reference axis as well. The first-generation of TS required manual calibration and measurement, but the new generation of TS, i.e., a robotic total station (RTS), integrates an axial stepper motor, a TS, and an automatic target alignment and identification algorithm. Therefore, it achieves automated structural displacement measurement. An RTS has been adopted for bridge and tunnel displacement measurements (Zhou et al., 2020a; Yu et al., 2017; Psimoulis and Stiros, 2007; Stiros and Psimoulis, 2012), and it can achieve a millimeter-level displacement measurement accuracy. However, it has a limited sampling rate of up to 20 Hz and is not suitable for long-term continuous displacement monitoring.

3. Structural displacement sensing techniques using multi-mode sensor fusion

Because all the sensors discussed in section 2 have limitations, extensive efforts have been made to combine multi-mode sensors to obtain better structural displacement estimations. Most sensor-fusion applications have combined an accelerometer with other sensors such as strain sensors and vision cameras, but the fusion applications of strain sensors and an inclinometer, an LDV and LiDAR, an LDV and a vision camera, and a vision camera and LiDAR have also been explored.

3.1. Fusion of accelerometer with other sensors

Aside from their inability to estimate low-frequency displacements, accelerometers perform well in almost every respect, as shown in Table 1. Therefore, combining an accelerometer with other sensors is straightforward, with the accelerometer determining the high-frequency displacement and the other sensor determining the low-frequency displacement.

3.1.1. General framework

The fusion of accelerometers and other sensors has been extensively studied, and the general framework of this fusion using a Kalman or FIR filter is shown in Fig. 2.

(a) Multi-rate Kalman filter

A multi-rate Kalman filter (Lee et al., 2010) has commonly been used in previous studies on data fusion-based structural displacement estimation (Zhu et al., 2020; Zhang et al., 2023), and its overall working principle is briefly introduced here. Let $\dot{x}_k$ and x_k be the true velocity and displacement, respectively, at the kth time step. Then, a discrete state space model for the acceleration–displacement relationship can be expressed as follows:

$$\boldsymbol{x}_k = \boldsymbol{A}(\Delta t_a)\boldsymbol{x}_{k-1} + \boldsymbol{B}(\Delta t_a)a_{k-1} + \boldsymbol{B}(\Delta t_a)w_{k-1} \tag{12}$$

$$u_k = \boldsymbol{H}x_k + v_k \tag{13}$$

$$\boldsymbol{A}(\Delta t_a) = \begin{bmatrix} 1 & \Delta t_a \\ 0 & 1 \end{bmatrix}, \boldsymbol{B}(\Delta t_a) = \begin{bmatrix} \frac{\Delta t_a^2}{2} \\ \Delta t \end{bmatrix}; \boldsymbol{H} = [1 \quad 0] \tag{14}$$

where $\boldsymbol{x}_k$ is the state vector $\{x_k, \dot{x}_k\}^T$, and a_{k-1} andu_k are the measured acceleration and displacement, respectively. w_{k-1} and v_k are the acceleration and displacement noises, respectively, and their variances are denoted by q and r, respectively. Δt_a is the time interval of the acceleration measurement. Based on this model, a multi-rate Kalman filter is formulated for displacement estimation using synchronous acceleration and displacement measurements. The state vector is predicted as $\hat{\boldsymbol{x}}_k^-$ using the estimated state vector and measured acceleration at the (k-1)th time step ($\hat{\boldsymbol{x}}_{k-1}^+$ and a_{k-1}, respectively):

$$\hat{\boldsymbol{x}}_k^- = \boldsymbol{A}(\Delta t_a)\,\hat{\boldsymbol{x}}_{k-1}^+ + \boldsymbol{B}(\Delta t_a)a_{k-1} \tag{15}$$

and the covariance matrix of the error in $\hat{\boldsymbol{x}}_k^-$ ($\hat{\boldsymbol{P}}_k^-$) is calculated as follows:

$$\hat{\boldsymbol{P}}_k^- = \boldsymbol{A}(\Delta t_a)\hat{\boldsymbol{P}}_{k-1}^+\boldsymbol{A}^T(\Delta t_a) + q\boldsymbol{B}(\Delta t_a)\boldsymbol{B}^T(\Delta t_a) \tag{16}$$

where $\hat{\boldsymbol{P}}_{k-1}^+$ is the covariance matrix of the error in $\hat{\boldsymbol{x}}_{k-1}^+$. If the displacement measurement (u_k) is available, $\hat{\boldsymbol{x}}_k^-$ is corrected to $\hat{\boldsymbol{x}}_k^+$, and the covariance matrix of the error in $\hat{\boldsymbol{x}}_k^+$ ($\hat{\boldsymbol{P}}_k^+$) is calculated accordingly,

$$\hat{\boldsymbol{x}}_k^+ = (\boldsymbol{I} - \boldsymbol{K}\boldsymbol{H})\hat{\boldsymbol{x}}_k^- + \hat{\boldsymbol{P}}_k^-\boldsymbol{H}^T\left(\boldsymbol{H}\hat{\boldsymbol{P}}_k^-\boldsymbol{H}^T + r\right)^{-1}u_k \tag{17}$$

$$\hat{\boldsymbol{P}}_k^+ = \left(\boldsymbol{I} - \hat{\boldsymbol{P}}_k^-\boldsymbol{H}^T\left(\boldsymbol{H}\hat{\boldsymbol{P}}_k^-\boldsymbol{H}^T + R\right)^{-1}\boldsymbol{H}\right)\hat{\boldsymbol{P}}_k^- \tag{18}$$

If the displacement measurement is not available, the following is used:

$$\hat{\boldsymbol{x}}_k^+ = \hat{\boldsymbol{x}}_k^-;\ \hat{\boldsymbol{P}}_k^+ = \hat{\boldsymbol{P}}_k^- \tag{19}$$

Table 1
Comparison of different sensors used for structural displacement estimation.

Sensors		Measurement Accuracy	Sampling rate	Stationary installation location	Measurement direction	Multi-point measurement	Long-term monitoring	Computational efficiency	Other limitations
Contact	LVDT (Nassif et al., 2005; Santhosh and Roy, 2017)	High	>100 Hz	Yes	Line of sight (LOS)	No	No	Low	Small-scale structures
	Accelerometer (Lee et al., 2010; Gomez et al., 2018)	High	>100 Hz	No	3D	No	Yes	Low	High-frequency displacement
	Strain sensor (Shin et al., 2012; Zhang et al., 2018a)	Low	>100 Hz	No	V/H	Yes	No	Low	Pre-knowledge of a target structure
	Inclinometer (Hou et al., 2005)	Low	>100 Hz	No	V/H	Yes	Yes	Low	Simple beam-type structure
	Connecting pip (Liu et al., 2015; Zhou et al., 2021)	Medium	<20 Hz	Yes	V	No	Yes	Low	Cumbersome installation
	Optical fiber sensor (Ramakrishnan et al., 2016)	High	>100 Hz	No	LOS	No	Yes	Low	Relative displacement
	GNSS (Tamura et al., 2002)	Low	<20 Hz	No	3D	No	Yes	Low	Multi-pathing issue
Noncontact	Stationary vision camera (Feng et al., 2015; Luo and Feng, 2018)	Medium	>100 Hz	Yes	2D	Yes	No	High	Sensitive to illumination
	Vision camera on target structure (Yu and Zhang, 2020)	Medium	>100 Hz	No	2D	No	Yes	High	
	Vision camera on a drone (Yoon et al., 2018; Weng et al., 2021)	Medium	>100 Hz	No	2D	Yes	No	High	
	Fixed radar (Zhang et al., 2020; Gentile and Bernardini, 2008, 2010)	High	>100 Hz	Yes	LOS	Yes	No	Low	Manual calibration, phase wrapping
	Radar on a target structure (Guan et al., 2017, 2018)	High	>100 Hz	No	LOS	No	Yes	Low	
	LDV (Reu et al., 2017; Toyoshima et al., 1994)	High	>100 Hz	Yes	LOS	No	No	Low	Reflector required
	LTS (Zhuojiang et al., 2021)	High	>100 Hz	Yes	LOS	No	No	Low	
	LiDAR (Lee et al., 2019; Lee and Kim, 2022; Park et al., 2007)	Low	<100 Hz	Yes	3D	Yes	No	High	–
	Level (Zhou et al., 2021; Yu and Zhang, 2020)	High	Manual	Yes	V	No	No	High	Leveling rod required
	TS (Zhou et al., 2020a; Yu et al., 2017)	High	<20 Hz	Yes	2D	Yes	No	High	Target required

Note that there are several limitations, and a few attempts have been made to address these. For example, Xu et al. combined a multi-rate Kalman filter with maximum likelihood estimation (MLE) to automatically estimate the values of q and r (Xu et al., 2017); Kim et al. revised the state-space mode to explicitly consider the acceleration bias (Kim et al., 2014), and this work was further improved by proposing a two-stage Kalman filter (Kim et al., 2016b); Ma et al. revised the multi-rate Kalman filter to make it suitable for fusing asynchronous measurements (Ma et al., 2022b).

(b) Finite impulse response (FIR) filter

FIR filter-based fusion for structural displacement estimation has also been extensively studied in previous works (Park et al., 2013b; Ma et al., 2021), and its overall working principle is briefly introduced here. With acceleration (a) and displacement (u) measurements available within a given time window $[(k - N)\Delta t, (k + N)\Delta t]$, the displacement can be estimated as follows:

$$\boldsymbol{u}^* = (\Delta t)^2\left(\boldsymbol{L}^T\boldsymbol{L}+\lambda^2\boldsymbol{I}\right)^{-1}\boldsymbol{L}^T\boldsymbol{L}_a\boldsymbol{a} + \lambda^2\left(\boldsymbol{L}^T\boldsymbol{L}+\lambda^2\boldsymbol{I}\right)^{-1}\boldsymbol{u};\ \boldsymbol{L} = \boldsymbol{L}_a\boldsymbol{L}_c \tag{20}$$

$$\boldsymbol{u}^* = \begin{bmatrix} u^*(k-N) \\ \vdots \\ u^*(k+N) \end{bmatrix}; \boldsymbol{u} = \begin{bmatrix} u(k-N) \\ \vdots \\ u(k+N) \end{bmatrix}; \boldsymbol{a} = \begin{bmatrix} a(k-N+1) \\ \vdots \\ a(k+N-1) \end{bmatrix} \tag{21}$$

where u^* is the estimated displacement; Δt is the time interval of the measurements; and λ is the regularization factor. $\boldsymbol{L}_c$ and $\boldsymbol{L}_a$ denote a second-order differential operator matrix and weighting matrix, respectively. More details on the derivation of Equation (20) can be found in Lee et al. (2010). Because the displacement estimation has the best performance at the center of the time window, only the displacement estimated at the center ($u^*(k)$) is retained:

$$u^*(k) = \boldsymbol{C}_H\boldsymbol{a} + \boldsymbol{C}_L\boldsymbol{u} \tag{22}$$

where $\boldsymbol{C}_H$ and $\boldsymbol{C}_L$ are the $(N+1)^{th}$ rows of matrices $\{(\Delta t)^2(\boldsymbol{L}^T\boldsymbol{L}+\lambda^2\boldsymbol{I})^{-1}\boldsymbol{L}^T\boldsymbol{L}_a\}$ and $\{\lambda^2(\boldsymbol{L}^T\boldsymbol{L}+\lambda^2\boldsymbol{I})^{-1}\}$, respectively. Note that $\boldsymbol{C}_H$ is a combination of a double integrator and high-pass filter, and $\boldsymbol{C}_L$ is a low-pass filter. Therefore, the final displacement is estimated by combining the low-frequency displacement from $\boldsymbol{u}$ and high-frequency displacement from $\boldsymbol{a}$, as shown in Fig. 12. Note that other different variants of the FIR filter have been proposed (Park et al., 2018; Hong et al., 2010, 2013), but the basic working principles are similar to those of the FIR filter.

3.1.2. Sensor-fusion examples

Accelerometers have been used in combination with inclinometers, vision cameras, GNSSs, strain sensors, and millimeter wave radars. Most of the existing studies mainly focused on the fusion of the initial

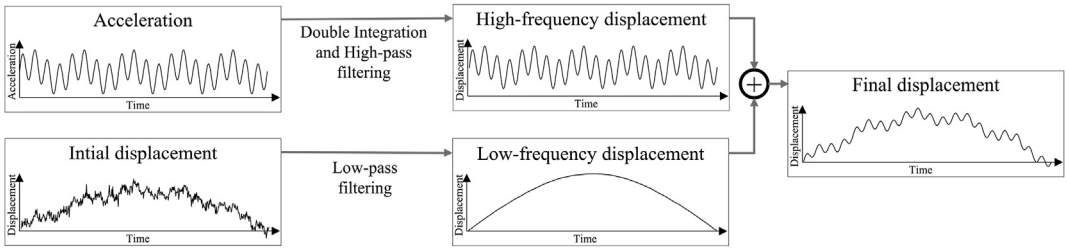

Fig. 12. Overview of improved structural displacement estimation using FIR-filter-based fusion of acceleration and initial displacement.

displacement from one of these sensors and the acceleration from the accelerometer. For example, Zhu et al. (2020) estimated low-sampling-rate and low-accuracy displacements using strain measurements and then fused these strain-based displacements with high-sampling-rate acceleration measurements using a multi-rate Kalman filter to obtain the final displacement with a high sampling rate and high accuracy for high-rise buildings. Zhou et al. (2022) performed similar work but an FIR filter was adopted instead of a Kalman filter. The fusion of the vision-based displacement and acceleration was explored by Park et al. (2018) using an FIR filter, and by Chang et al. (Chang and Xiao, 2010) and Xu et al. (2019) using a multi-rate Kalman filter. Ozdagli et al. (2017) estimated displacements for cantilever-type railway bridge piers through the fusion of the inclinometer-based displacement and acceleration. Xu et al. (2017) and Koo et al. (2017) explored the fusion of the GNSS-based displacement and acceleration using an MLE-enhanced multi-rate Kalman filter and a two-stage multi-rate Kalman filter, respectively.

However, a low sampling rate and low accuracy are not the only issues when estimating the displacement using these sensors. Another trend in multi-sensor fusion-based structural displacement estimation is to first use the acceleration to assist in the displacement-estimation process of these sensors, and then fuse the displacements from these sensors with the acceleration, as shown in Fig. 13. For example, when fusing the acceleration with strain gauge measurements, the strain-based displacement is usually estimated with a mode-superposition algorithm. However, this algorithm requires mode shapes and the neutral axis location of a target structure. Park et al. (2013b) eliminated this requirement by using simplified mode shapes and introducing a scale factor to estimate the neutral axis location and compensate for the displacement estimation error induced by the discrepancy between the simplified and true mode shapes. The unknown scale factor was pre-estimated using the initial strain and acceleration measurements. Later, Ma et al. (Ma et al., 2021; Ma and Sohn, 2019) combined a recursive least square algorithm and an FIR filter to simultaneously estimate the unknown scale factor and displacement at each time step.

With the help of an acceleration measurement, Chan et al. (2006), and Moschas and Stiros (2011), first denoised the GNSS-based displacement using the combination of Empirical mode decomposition (EMD) and an adaptive filter, and the multi-level filtering algorithm, respectively. Then, the denoised GNSS-based displacements were combined with the acceleration for the final displacement estimation. A similar attempt was made by Kim and Sohn (2020). A modified heuristic drift reduction algorithm was first applied to reduce the low-frequency error in the original GNSS-based displacement and obtain an enhanced GNSS-based displacement, which was further fused with an acceleration measurement using a two-stage multi-rate Kalman filter to estimate the final displacement.

Fig. 14 shows a structural displacement estimation technique that uses asynchronous measurements from a vision camera and an accelerometer (Ma et al., 2022b). A scale factor is first calculated automatically from the initial acceleration and vision measurements. Next, a low-sampling-rate vision-based displacement is estimated using an improved feature matching algorithm that includes acceleration-aided ROI updating and mismatch rejection. Finally, the vision-based displacement is fused with the high-sampling-rate acceleration using an adaptive multi-rate Kalman filter to estimate the final displacement with improved accuracy and an increased sampling rate. The technique was further enhanced by replacing a feature-matching algorithm with hybrid computer vision to further improve the displacement estimation accuracy, with only a slight sacrifice in efficiency (Ma et al., 2022c).

A similar framework has been adopted for structural displacement estimation using a millimeter-wave radar and an accelerometer collocated at the displacement estimation points of a target structure (Ma et al., 2022d, 2023a). Using the initial radar and acceleration measurements, the best target for the millimeter-wave radar was automatically selected from the surroundings of the target structure, and the direction

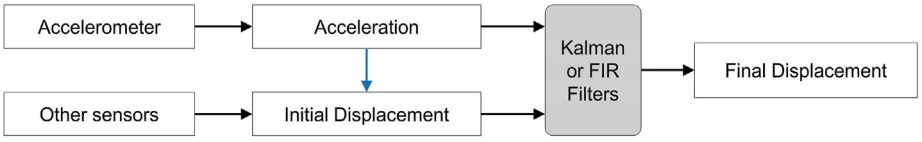

Fig. 13. Improved framework for structural displacement estimation through fusion of accelerometer with other sensors.

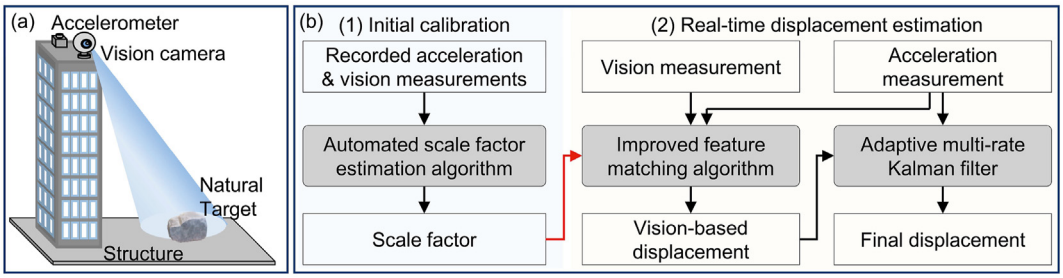

Fig. 14. Overview of structural displacement estimation by fusing an accelerometer and a vision camera (Ma et al., 2022b): (a) sensor setup and (b) overall flowchart.

conversion factor was automatically estimated for this target. Afterward, the radar-based displacement was estimated in real-time from the best target with the help of the developed acceleration-aided adaptive phase-unwrapping algorithm. The radar-based displacement was finally fused with the acceleration measurement using an FIR filter to estimate the final displacement with improved accuracy.

3.2. Other sensor-fusion examples

In addition to the fusion of accelerometers and other sensors, other sensor-fusion combinations have also been studied. Sun et al. fused multiple strain sensors and inclinometers for bridge displacement estimation (Sun et al., 2020), and Kim et al. fused the LiDAR-based displacement and LDV-based velocity using a Kalman filter for improved displacement estimation (Kim and Sohn, 2017; Kim et al., 2016a). Efforts have also been made to combine a vision camera and an LDV installed on a drone (Nasimi and Moreu, 2021a, 2021b). The LDV measured the relative displacement between a target structure and the drone, and the 6-DOF motion of the drone was estimated using the vision camera and an artificial target placed at a stationary location. Finally, the absolute displacement of the target was estimated by compensating for the errors induced by the drone motion. Note that the drone had to be close to the artificial target to ensure an accurate estimation of the 6-DOF motion of the drone, and that the target structure had to have a vertically flat surface, both of which may not be easy to satisfy in most applications. The fusion of a vision camera and LiDAR was explored by Lee et al. (2022b). The displacement of a target structure in the image plane was first estimated in pixel units using the vision camera, which was then converted into length units using the transformation relationship between the image and world coordinates developed by the LiDAR.

4. Applications and challenges

4.1. Domain-specific applications

The displacement-estimation techniques discussed in the previous two sections have been applied to a wide range of structural types, including buildings and bridge structures.

4.1.1. Building structures

Table 2 summarizes the studies on displacement estimation for high-rise building structures. RTK-GNSS was applied to estimate the displacement of a 118-m-high steel tower under wind loadings (Tamura et al., 2002). A vision camera installed on a drone was used to estimate a large dynamic structural displacement of the 247-m-high ThyssenKrupp elevator tower excited using an active mass damper (Weng et al., 2021). The displacements of the 454-m-high Canton Tower were first estimated using strain sensors (Xia et al., 2014) under typhoon Usagi and then using strain sensors and an accelerometer (Zhu et al., 2020) under typhoon Koppu and environmental temperature variation. The fusion of strain sensors and an accelerometer has been applied for the displacement estimation of a 600-m-high-skyscraper (Zhou et al., 2022).

Other building structures that are not considered high-rise buildings have weak vibrations under ambient and wind excitations, and therefore no existing studies are available on their displacement estimation. However, accelerometers are commonly installed on these building structures, and their displacements during earthquakes have been estimated from acceleration measurements.

4.1.2. Bridge structures

Displacement estimation has been extensively studied for large-span bridges, and these studies are listed in Table 3. RTK-GNSS was applied to estimate the displacement of the 720-m-long Hakucho Suspension Bridge under wind loadings (Nakamura, 2000). A connecting pipe system was used to estimate the multi-point displacement of the 820-m-long Nanxi Suspension Bridge under environmental temperature variation and vehicle loadings (Liu et al., 2015). Vision cameras were adopted to estimate the displacements of the 451-m-long Manhattan Bridge (Luo and Feng, 2018) and a 100-m-long arch bridge (Yu and Zhang, 2020) under normal operation and controlled truck excitations, respectively. Radars were applied to estimate the displacements of the 448-m-long Stonecutters Bridge (Zhang et al., 2018b) under wind and vehicle loadings, the 1377-m-long Tsing Ma Bridge (Zhang et al., 2018b) under train loadings, and the 1200-m-long Dasha suspension bridge (Zhang et al., 2020) under controlled truck excitations. The displacements of the first two bridges were also estimated using vision cameras under controlled truck and normal operations, respectively. The fusion of different sensors has also been used for the displacement estimation of large-span bridges. A GNSS and an accelerometer were adopted to estimate the displacements of the 300-m-long Yeongjong Grand Bridge (Kim et al., 2018), 280-m-long Qingfeng Bridge (Kim and Sohn, 2020), and 704-m-long San Francisco–Oakland Bay Bridge (Kim and Sohn, 2020) under normal operation. FBG strain sensors and an accelerometer were applied to estimate the displacement of the 250-m-long Sorok Bridge under controlled vehicle loadings (Park et al., 2013b).

Table 4 lists the studies on short/medium-span bridge displacement estimations. Strain sensors were used for estimating the displacements of steel and concrete girder bridges under truck loadings (Helmi et al., 2015). The displacements of prestressed-concrete bridges were estimated using connecting pipe systems under truck loadings over the short term (Zhou et al., 2021) and long term (Lee et al., 2022a). The displacements of a prestressed-concrete bridge were also estimated using a vision camera (Lee et al., 2020) and LiDAR (Lee et al., 2019) during the construction stage. Accelerometers were used to estimate the dynamic displacements of the piers of a timber railway bridge (Gomez et al., 2018; Moreu et al., 2016), and a microwave radar was used to estimate the dynamic displacement of a timber suspension pedestrian bridge (Guan et al., 2017). Studies have also been done on the fusion of different sensors to estimate the displacements of short/medium-span bridges, including the fusion of an LDV and a LiDAR for a highway bridge (Kim et al., 2016a), the fusion of a vision camera and a LiDAR for a railway

Table 2
Summary of studies on high-rise building-displacement estimation.

Structure	Height (m)	Sensor(s) used	Reference sensor	Excitation	Accuracy	Sampling rate (Hz)
Steel tower	118	RTK-GNSS (Tamura et al., 2002)	N/A	Wind	N/A	10
ThyssenKrupp elevator tower	247	Vision camera (on a drone) (Weng et al., 2021)	Velocity sensor	Excited using an active mass damper	RMSE of 2.4 cm	25
454-m-high Canton Tower	454	Strain sensor & Accelerometer (Zhu et al., 2020)	RTK-GNSS	Typhoon Usagi	RMSE = 1.081 cm	5
		Strain sensor (Xia et al., 2014)	RTK-GNSS	Temperature variation and Typhoon Koppu	Centimeter-level	1
600-m-high-skyscraper	600	Strain sensor & Accelerometer (Zhou et al., 2022)	Microwave radar	Typhoon Kompasu	Millimeter-level	1
Tianjin radio and television tower	415	RTK-GNSS (Xiong et al., 2022)	N/A	Normal operation	N/A	10

Table 3
Summary of studies on long-span bridge displacement estimation.

Bridge	Span length (m)	Sensor(s) used	Reference sensor	Excitation	Accuracy	Sampling rate (Hz)
Hakucho Suspension Bridge	720	RTK-GNSS (Nakamura, 2000)	N/A	Wind	N/A	1
Nanxi Suspension Bridge	820	Connecting pipe (Liu et al., 2015)	Simulation	Temperature variation and vehicle loadings	N/A	0.5
Manhattan Bridge	451	Vision camera (Luo and Feng, 2018)	N/A	Normal operation	N/A	60
Arch bridge	100	Vision camera (Yu and Zhang, 2020)	Inclinometer and level	Controlled trucks	$\leq$ 0.2 mm	1
Stonecutters Bridge	448	Vision camera (Ye et al., 2013)	N/A	Controlled trucks	N/A	5
Tsing Ma Bridge	1377	Ground-based radar (Zhang et al., 2018b)	GNSS	Trains	Consistent with GNSS	10
Stonecutters Bridge	448		N/A	Wind and vehicle	N/A	100
Tsing Ma Bridge	1377			Trains		
Dasha suspension bridge	1200	Ground-based radar (Zhang et al., 2020)	Connecting pipe and Camera	Controlled trucks	Consistent with reference	100
Yeongjong Grand Bridge	300	GNSS & Accelerometer (Kim et al., 2018)	LDV	Normal operation	RMSE of 1.55 mm	100
Qingfeng Bridge	280	GNSS & Accelerometer (Kim and Sohn, 2020)	LDV	Normal operation	RMSE of 5.08 mm	100
San Francisco-Oakland Bay Bridge	704				RMSE of 5.44 mm	
Sorok Bridge	250	FBG strain sensor & Accelerometer (Park et al., 2013b)	LDV	Controlled trucks	Consistent with reference	Not mentioned

Table 4
Summary of studies on short/medium-span bridge-displacement estimation.

Bridges	Span length (m)	Sensor(s) used	Reference sensor	Excitation	Accuracy	Sampling rate (Hz)
Steel girder bridge	39.3	Strain sensor (Helmi et al., 2015)	LDV	A dump truck with a trailer	Not completely in agreement	500
Concrete box-girder bridge	14		LVDT	Several trucks	$\leq$ 8.18%	50
Piles of timber railroad bridges	14 (height)	Accelerometer (Moreu et al., 2016)	LVDT	Work trains	$\leq$ 0.45 mm ($\leq$ 13.6%)	100
	18 (height)	Accelerometer (Gomez et al., 2018)	Vision camera	Freight train	$\leq$ 1.6% (>0.9 Hz)	128
PSC box-girder bridge	16	Connecting pipe (Zhou et al., 2021)	Manual leveling (Vanicek et al., 1980)	Three-axle trucks	$\leq$ 13%	20
PSC box-girder bridge	Not mentioned	Connecting pipe (Lee et al., 2022a)	N/A	2-year monitoring	N/A	20
PSC railroad bridge	40	Vision camera (Lee et al., 2020)	Simulation and LiDAR (Lee et al., 2019)	During construction	N/A	1/60
		LiADR (Lee et al., 2019)	Simulation		$\leq$ 3.4 mm	1/15 days
Timber suspension pedestrian bridge	50	Radar (Guan et al., 2017)	Accelerometer	A person jumping	N/A	Not provided
Highway bridge	45	LDV and LiDAR (Kim et al., 2016a)	LDVT	Two 3-axel trucks	$\leq$ 0.07 mm	1280
Railroad bridge	40	Vision camera & LiDAR (Lee et al., 2022b)	LVDT	Trains	$\leq$ 0.1 mm	163
Steel box-girder pedestrian bridge	40	Accelerometer & strain gauge (Ma et al., 2021)	LDV	People jumping and walking	<0.09 mm	128
		Accelerometer & vision camera (Ma et al., 2022c)			<0.06 mm	100
		Accelerometer & millimeter wave radar (Ma et al., 2023a)			<0.04 mm	100

bridge (Lee et al., 2022b), and the fusion of an accelerometer with three different sensors (i.e., strain gauges, a vision camera, and a millimeter-wave radar) (Ma et al., 2021, 2022c, 2023a) for a steel box-girder pedestrian bridge.

4.1.3. Other structures

As listed in Table 5, displacements have also been estimated for structures other than bridges and building structures. GNSS was used to monitor the long-term displacements of the Eleonora D'Arborea Dam (Barzaghi et al., 2018) and Xilongchi Dam (Xi et al., 2022). A vision camera was used to estimate the displacement of a football stadium during normal operation. The fusion of strain sensors and accelerometers was used for the displacement estimation of a transmission tower under pseudo-static testing. The long-term displacement of a landslide was monitored using a GNSS (Pehlivan, 2022). An RTS (Zhou et al., 2020a) was used to estimate the long-term displacement of an underground tunnel. A vision camera was used to estimate the displacement of an underground drainage tunnel under normal operation. Displacement estimation for underwater structures (i.e., submerged floating tunnels) has also been studied through the fusion of strain sensors and accelerometers (Ma et al., 2022e, 2023b), but field applications have not yet been performed.

Table 5
Summary of studies on structural displacement estimation for structures other than bridges and building structures.

Structure	Sensor(s) used	Reference sensor	Excitation	Accuracy	Sampling rate (Hz)
Eleonora D'Arborea Dam	GNSS (Barzaghi et al., 2018)	Pendulums	Long term	N/A	1
Xilongchi Dam	GNSS (Xi et al., 2022)	N/A	Long term	N/A	Static
Football stadium	Vision camera (Khuc and Catbas, 2017b)	LVDT	Normal operation	±0.04 mm	60
Transmission tower	Strain sensor & Accelerometer (Zhang et al., 2023)	TS	Pseudo-static test	<5.4 mm	100
Landslide	GNSS (Pehlivan, 2022)	N/A	Long term	N/A	
Underground tunnel	RTS (Zhou et al., 2020a)	Level	Long term	N/A	Static
Underground drainage tunnel	Vision camera (Chen et al., 2020)	N/A	Normal operation	N/A	1/600

4.2. Discussion and challenges

4.2.1. Measurement accuracy

The measurement accuracy is very important for a mature measurement system and should be considered when selecting a sensor for structural displacement estimation. The measurement-accuracy requirement varies for different types of structures. Large-scale structures such as long-span bridges and high-rise buildings usually have at least centimeter-level displacements. Thus, a millimeter-level accuracy may be sufficient for these structures. Therefore, the fusion of a GNSS and an accelerometer (Kim and Sohn, 2020; Kim et al., 2018) seems to be a good option for these structures because it has sufficient accuracy, easy installation, and the ability to be used for long-term continuous monitoring. However, submillimeter accuracy is required for small-scale structures because their displacements are in the range of millimeters or less.

However, it is not simple to quantify the estimation accuracies of many sensors because they vary with the hardware setup and field conditions. For example, the displacement-estimation accuracy of a vision camera is sensitive to environmental conditions such as the lighting conditions and the atmospheric refraction and turbulence. Many factors such as the camera-to-target distance and texture of a target differ with the application, but they have significant effects on the displacement-estimation accuracy. Moreover, the quantification of the displacement-estimation accuracy under field conditions is difficult. The displacement-estimation accuracy of any developed technique should be evaluated through comparisons with reference displacement measurements, but it is commonly difficult to obtain such reference displacements. As listed in Tables 2–5, although various techniques have been proposed and applied for structural displacement estimation, their accuracies were not well-evaluated. Most studies either compared the frequency spectra of the estimated displacement and acceleration measurement or qualitatively analyzed the consistency between the estimated displacement and applied loading.

4.2.2. Frequency range

The frequency range is also an important factor that should be considered when selecting a sensor for structural displacement estimation. The displacements of most civil structures are dominated by low-frequency (including pseudo static and static) components induced by the environmental temperature variation, vehicle loading, wind loading, etc. These play a vital role when using the displacement for safety-index evaluation (AASHTO, 2017; MLTM. Korea, 2010; MOHURD., 2020), bridge-loading tests (Lee et al., 2006; Vicente et al., 2015; Dong et al., 2020; Sun et al., 2021; Hester et al., 2017), damage detection (Feng and Feng, 2016), finite element model updating (Feng and Feng, 2015; Civera et al., 2020), etc. Therefore, the ability to estimate the low-frequency displacement is important for any sensor. As shown in Table 1 and discussed in section 2, with the exception of the accelerometer, the estimation of the low-frequency displacement is not difficult for the various sensors used. However, the accurate estimation of the low-frequency displacement is still challenging for most sensors. For example, a GNSS usually suffers from a multi-path issue, which causes low-frequency (<0.1 Hz) error in the GNSS-based displacement. Strain gauges have zero-drift for long-term monitoring (Lee et al., 2022c). Time-varying environmental conditions such as the temperature. Light conditions, atmospheric refraction, and turbulence will cause a low-frequency error in vision-based displacement (Luo et al., 2020).

Apart from these low-frequency displacements, many structures also have high-frequency displacements as a result of resonance. Thus, the sampling frequency should be large enough to include all the high-frequency components. The importance mode frequencies of civil infrastructures are usually below 50 Hz. Thus, a sampling rate of 100 Hz is sufficient (Feng and Feng, 2018). As listed in Tables 2–5, high-sampling displacement measurements are challenging for some sensors because of hardware limitations (e.g., a GNSS, a connecting pipe, or an RTS) or high computational costs (e.g., a vision camera or LiDAR). However, the fusion of one of these sensors with an accelerometer seems to be a good solution to address the high-sampling displacement measurement issue, as reported in previous studies (Ma et al., 2022b; Kim et al., 2018).

4.2.3. Multi-point displacement measurement

As previously mentioned, the displacement response has been used for bridge-loading tests (CEN. Eurocode 1, 2003; Lee et al., 2006; Vicente et al., 2015; Dong et al., 2020; Sun et al., 2021), structural damage detection (Hester et al., 2017), modal identification (Feng and Feng, 2016, 2017; Kim et al., 2013; Bhowmick and Nagarajaiah, 2020), and finite element model updating (Jiao et al., 2021; Feng and Feng, 2015). In most of these studies, the displacements at multiple locations on a target structure are needed. The multi-point displacements of target structures can be simultaneously estimated using a radar, vision camera, or LiDAR (Zhang et al., 2020; Gentile and Bernardini, 2010; Bhowmick and Nagarajaiah, 2022) installed at a stationary location. However, securing such an installation location may not be easy, especially for long-term continuous displacement estimation. The installation of these sensors at a displacement estimation point of a target structure eliminates the need for such a stationary installation but sacrifices the ability to obtain simultaneous multi-point displacement estimations. Moreover, multi-point displacement estimations commonly have lower displacement-estimation accuracy. For example, when estimating the displacements at multiple locations of a target structure using a vision camera, all of the locations must be visible in the field of view (FOV) of the camera. However, a wide FOV requires either a long distance between the camera and target structure or a short focal length for the camera. Both of these will cause a large-scale factor and poor displacement-estimation performance. Note that simultaneous multi-point displacement estimation can also be achieved using a synchronized system that includes multiple sensors (Shajihan et al., 2022; Lydon et al., 2018), where each sensor module only estimates the displacement at a single point. However, the cost will also increase.

4.2.4. Multi-directional displacement measurement

Short/medium span bridges commonly vibrate only in the vertical direction. Thus, monitoring the vertical displacement is sufficient. Vertical displacement monitoring may be sufficient for cable-stayed bridges, beam-type bridges, and arch bridges, but both the vertical and horizontal displacements need to be monitored for suspension bridges (Mot. Jt/, 2022). However, all the studies listed in Table 5 estimated vertical bridge displacements alone. For building structures, the vertical displacement

can be ignored, but the horizontal displacements in two directions should be monitored.

Most of the sensors mentioned in section 2 can only estimate the displacement in a single direction. For example, LVDT, LDV, LTS, radar, and optical fiber sensors only estimate the LOS displacement, while connecting pipe, level, and inclinometer sensors can only estimate the vertical displacement. Some sensors can estimate two-dimensional displacements, including vision cameras for in-plane 2D displacements, strain sensors for the two horizontal displacements of a building, and an RTS for one vertical and one horizontal displacement. Only a few sensors such as a GNSS, LiDAR, and an accelerometer can estimate 3D displacements. However, an accelerometer can only estimate the high-frequency displacement, while the other three sensors suffer from a low-accuracy issue in practical applications. Note that a few attempts have been made to estimate 3D displacements using a vision camera. However, either a binocular camera (Shao et al., 2021, 2022) or an additional projector (Felipe-Sesé et al., 2014) is required, and these techniques are not suitable for practical applications because of the long camera-to-target distances required. In addition, 3D displacements and 3D rotations can be simultaneously estimated using a monocular camera and an artificial target, but high-accuracy estimation requires short camera-to-target distances.

4.2.5. Long-term continuous displacement monitoring

As shown in section 4.1, domain-specific applications mainly focus on short-period displacement surveys. Although a few attempts have been made for long-term displacement monitoring using GNSSs, connect pipe systems, or vision cameras, their displacement monitoring performances have not been well validated. For long-term continuous displacement monitoring, the displacement estimation techniques must have robustness to time-varying operational and environmental conditions. For example, a radar, laser-based sensor, vision camera, level, and TS require a clear LOS between the target and sensor, which may not be guaranteed in some applications. The displacement estimation performance of a vision camera is sensitive to the inevitable variation in the daily illumination level, and vision cameras cannot operate under poor illumination conditions such as at night. The effects of atmospheric refraction and turbulence on light or a laser beam propagating through the air may be ignored for a short period but have to be considered in long-term continuous displacement monitoring. In addition, extreme weather conditions such as rain, snow, and fog have effects on the displacement-estimation accuracies of many sensors, and they have to be considered in long-term continuous displacement monitoring. In addition to the robustness to time-varying operational and environmental conditions, the ability to perform real-time displacement estimation is also important. However, real-time estimation may not be feasible for sensors such as vision cameras, which have a high computational cost for structural displacement estimation.

4.2.6. Seismic-induced structural displacement estimation

It is essential to determine the structural displacement when assessing the post-earthquake damage to civil infrastructures. However, few of the techniques mentioned in section 2 can be applied to seismic-induced-displacement estimation. LVDT, RTK-GNSS, and connecting pipe systems require a stationary reference point, while a vision camera, ground-based radar, laser-based sensor, level, and TS must be installed at a stationary location, neither of which is possible in seismic-induced-displacement estimation. Strain sensors and inclinometers cannot estimate the rigid body translation of a target structure. Note that while inclinometers were employed previously to estimate building displacement under seismic loading, its emphasis was on the inter-story drift (Hou et al., 2018). A single GNSS can be used for seismic-induced-displacement estimation, but only centimeter-level accuracy can be achieved. Currently, accelerometers are the most commonly used sensors for seismic-induced-displacement estimation. However, measurement noise and acceleration baseline shifts interfere with low-frequency displacement estimation. Although several baseline correction techniques have been proposed, they all require some ad-hoc thresholds. High-pass filters have also been adopted to remove the low-frequency drift, but the low-frequency component of the real structural response is also removed.

4.2.7. Other practical issues in displacement estimation for civil infrastructures

In addition to the aforementioned considerations, other issues should be considered for the practical application of displacement-estimation techniques to civil infrastructures. The sensor installation location is the first thing that should be considered for displacement estimation in the field. The sensors used in the contact-type displacement-estimation techniques discussed in section 2.1, including an accelerometer, an LVDT, inclinometer, a strain sensor, a connecting pipe, an optical fiber sensor, and a GNSS, have to be installed at displacement-estimation points. The sensors used in the noncontact displacement-estimation techniques discussed in section 2.2 are commonly installed at a fixed location because most of the current studies focus on short-term displacement surveys and prefer noncontact measurements. It should be noted some radar-based, laser-based, and vision-based techniques require the installation of an artificial target or a reflector at the displacement measurement location, and therefore are not fully noncontact techniques. In addition, as discussed in section 4.2.3, in order to simultaneously estimate the structural displacements at multiple locations using a single sensor such as a vision camera or radar, it has to be installed at a fixed location.

However, securing a fixed installation location can be challenging for field applications, especially for long-term continuous displacement estimation, because these sensors can be stolen or damaged when they are permanently installed in a public open space. Getting permission to install these sensors on privately owned properties can also be difficult. For long-term continuous displacement monitoring, it is preferable to install sensors on the target measurement points rather than off-site. However, the installation of sensors at displacement-estimation points results in additional problems. For example, when installing vision cameras or radars on a target structure for displacement estimation, multiple targets are commonly available in the FOV of the vision camera or radar, and the automatic selection of a good target can be a problem. In addition, a tiny structural rotation will introduce large errors in the estimated displacements.

Moreover, the data measured by any sensor should be transmitted to users, and sensors need power for their sensing, data processing, and transmission operations. Therefore, the methods used for transmitting data and supplying power should also be considered. A wired monitoring system can provide relatively stable data transmission, and the power supply may not be a problem even for long-term continuous monitoring. However, a wired monitoring system is expensive to install and maintain (Lynch, 2007). It has become increasingly popular in the field of SHM to use wireless networking because it is less costly, and several studies have been conducted to develop wireless displacement sensors (Shajihan et al., 2022; Lydon et al., 2018; Hou and Wu, 2019; Ozdagli et al., 2018; Park et al., 2014). However, wireless sensors have several problems, including problems with time synchronization and decentralized data processing, which directly affect the long-term reliability of data access via wireless networks. Moreover, the power supply is a major issue when using wireless displacement sensors for long-term continuous monitoring, but the problem may be addressed by developing self-powered wireless displacement sensors using energy harvesting (Wu et al., 2022).

5. Conclusion

This paper presented a comprehensive review of structural displacement sensing techniques, particularly focusing on those used for civil infrastructures. The general working principles of structural displacement sensing techniques using thirteen different sensors were first

reviewed, followed by a review of multi-sensor fusion-based structural displacement sensing techniques. The domain-specific applications of these techniques were then reviewed, and the remaining challenges were discussed in detail. Although the potential of these displacement-estimation techniques has been validated in various field applications, the following issues should be addressed:

- o The development of robust real-time displacement-estimation techniques for long-term continuous monitoring;
- o The development of low-cost wireless and self-powered displacement sensors;
- o The development of six-degree-of-freedom structural displacement estimation techniques;
- o The development of seismic-induced structural displacement estimation techniques.

In addition, other physical quantities like rotation, strain, acceleration, wind speed, temperature, and humidity are also important for structural health monitoring, and simultaneous measurements of multiple physical quantities should be considered in future work.

Declaration of competing interest

The authors declare that they have no known competing financial interests or personal relationships that could have appeared to influence the work reported in this paper.

Acknowledgment

This work was supported by National Research Foundation of Korea (NRF) grants funded by the Korean government (MSIT) (No. 2017R1A5A1014883 and No. 2022R1C1C2008186).

References

AASHTO, 2017. Aashto LRFD Bridge Design Specifications. the American Association of State Highway and Transportation Officials, Washington, D.C.
Barzaghi, R., Cazzaniga, N.E., De Gaetani, C.I., Pinto, L., Tornatore, V., 2018. Estimating and comparing dam deformation using classical and GNSS techniques. Sensors 18 (3), 756.
Bhowmick, S., Nagarajaiah, S., 2020. Identification of full-field dynamic modes using continuous displacement response estimated from vibrating edge video. J. Sound Vib. 489, 115657.
Bhowmick, S., Nagarajaiah, S., 2022. Spatiotemporal compressive sensing of full-field Lagrangian continuous displacement response from optical flow of edge: identification of full-field dynamic modes. Mech. Syst. Signal Process. 164, 108232.
Blais, F., 2004. Review of 20 years of range sensor development. J. Electron. Imag. 13 (1), 231–243.
Bonopera, M., Chang, K.C., Chen, C.C., Lee, Z.K., Sung, Y.C., Tullini, N., 2019. Fiber bragg grating–differential settlement measurement system for bridge displacement monitoring: case study. J. Bridge Eng. 24 (10), 05019011.
CEN. Eurocode 1, 2003. Actions on Structures - Part 2: Traffic Loads on Bridges. European Committee for Standardization, Brussels, Belgium.
Chan, W.S., Xu, Y.L., Ding, X.L., Dai, W.J., 2006. An integrated GPS–accelerometer data processing technique for structural deformation monitoring. J. Geodes. 80 (12), 705–719.
Chan, T.H.T., Ashebo, D.B., Tam, H.Y., Yu, Y., Chan, T.F., Lee, P.C., et al., 2009. Vertical displacement measurements for bridges using optical fiber sensors and CCD cameras — a preliminary study. Struct. Health Monit. 8 (3), 243–249.
Chang, C.C., Xiao, X.H., 2010. An integrated visual-inertial technique for structural displacement and velocity measurement. Smart Struct. Syst. 6 (9), 1025–1039.
Chen, S.Z., Wu, G., Xing, T., 2017a. Deflection monitoring for a box girder based on a modified conjugate beam method. Smart Mater. Struct. 26 (8), 085034.
Chen, J.G., Davis, A., Wadhwa, N., Durand, F., Freeman, W.T., Büyüköztürk, O., 2017b. Video camera–based vibration measurement for civil infrastructure applications. J. Infrastruct. Syst. 23 (3), B4016013.
Chen, I.H., Ho, S.C., Su, M.B., 2020. Computer vision application programming for settlement monitoring in a drainage tunnel. Autom. ConStruct. 110, 103011.
Civera, M., Fragonara, L.Z., Surace, C., 2020. A computer vision-based approach for non-contact modal analysis and finite element model updating. In: European Workshop on Structural Health Monitoring. Springer.
Corsetti, M., Fossati, F., Manunta, M., Marsella, M., 2018. Advanced SBAS-DInSAR technique for controlling large civil infrastructures: an application to the genzano di Lucania dam. Sensors 18 (7), 2371.
Dong, C.Z., Catbas, F.N., 2021. A review of computer vision–based structural health monitoring at local and global levels. Struct. Health Monit. 20 (2), 692–743.
Dong, C.Z., Celik, O., Catbas, F.N., 2019. Marker-free monitoring of the grandstand structures and modal identification using computer vision methods. Struct. Health Monit.- An Int. J. 18 (5–6), 1491–1509.
Dong, C.Z., Bas, S., Catbas, F.N., 2020. A portable monitoring approach using cameras and computer vision for bridge load rating in smart cities. J. Civ. Struct. Health Monit. 10 (5), 1001–1021.
Felipe-Sesé, L., Siegmann, P., Díaz, F.A., Patterson, E.A., 2014. Simultaneous in-and-out-of-plane displacement measurements using fringe projection and digital image correlation. Opt Laser. Eng. 52, 66–74.
Feng, D., Feng, M.Q., 2015. Model updating of railway bridge using in situ dynamic displacement measurement under trainloads. J. Bridge Eng. 20 (12), 04015019.
Feng, D., Feng, M.Q., 2016. Output–only damage detection using vehicle–induced displacement response and mode shape curvature index. Struct. Control Health Monit. 23 (8), 1088–1107.
Feng, D., Feng, M.Q., 2017. Identification of structural stiffness and excitation forces in time domain using noncontact vision-based displacement measurement. J. Sound Vib. 406, 15–28.
Feng, D., Feng, M.Q., 2018. Computer vision for SHM of civil infrastructure: from dynamic response measurement to damage detection – a review. Eng. Struct. 156, 105–117.
Feng, M.Q., Fukuda, Y., Feng, D., Mizuta, M., 2015. Nontarget vision sensor for remote measurement of bridge dynamic response. J. Bridge Eng. 20 (12), 04015023.
Gentile, C., Bernardini, G., 2008. Output-only modal identification of a reinforced concrete bridge from radar-based measurements. NDT E Int. 41 (7), 544–553.
Gentile, C., Bernardini, G., 2010. An interferometric radar for non-contact measurement of deflections on civil engineering structures: laboratory and full-scale tests. Struct. Infrastruct. Eng. 6 (5), 521–534.
Gindy, M., Vaccaro, R., Nassif, H., Velde, J., 2008. A state-space approach for deriving bridge displacement from acceleration. Comput. Aided Civ. Infrastruct. Eng. 23 (4), 281–290.
Gomez, F., Park, J.W., Spencer, B.F., 2018. Reference-free structural dynamic displacement estimation method. Struct. Control Health Monit. 25 (8), e2209.
Guan, S., Rice, J.A., Li, C., Li, Y., Wang, G., 2017. Structural displacement measurements using DC coupled radar with active transponder. Struct. Control Health Monit. 24 (4), e1909.
Guan, S., Bridge, J.A., Li, C., DeMello, N.J., 2018. Smart radar sensor network for bridge displacement monitoring. J. Bridge Eng. 23 (12), 04018102.
Guo, J., He, Y., Jiang, C., Jin, M., Li, S., Zhang, J., et al., 2021. Measuring micrometer-level vibrations with mmWave radar. IEEE Trans. Mobile Comput. 1.
Helmi, K., Taylor, T., Zarafshan, A., Ansari, F., 2015. Reference free method for real time monitoring of bridge deflections. Eng. Struct. 103, 116–124.
Hester, D., Brownjohn, J., Bocian, M., Xu, Y., 2017. Low cost bridge load test: calculating bridge displacement from acceleration for load assessment calculations. Eng. Struct. 143, 358–374.
Hofmann-Wellenhof, B., Lichtenegger, H., Collins, J., 2012. Global Positioning System: Theory and Practice. Springer Science & Business Media.
Hong, Y.H., Kim, H.K., Lee, H.S., 2010. Reconstruction of dynamic displacement and velocity from measured accelerations using the variational statement of an inverse problem. J. Sound Vib. 329 (23), 4980–5003.
Hong, Y.H., Lee, S.G., Lee, H.S., 2013. Design of the FEM-FIR filter for displacement reconstruction using accelerations and displacements measured at different sampling rates. Mech. Syst. Signal Process. 38 (2), 460–481.
Hou, S., Wu, G., 2019. A low-cost IoT-based wireless sensor system for bridge displacement monitoring. Smart Mater. Struct. 28 (8), 085047.
Hou, X., Yang, X., Huang, Q., 2005. Using inclinometers to measure bridge deflection. J. Bridge Eng. 10 (5), 564–569.
Hou, S., Zeng, C., Zhang, H., Ou, J., 2018. Monitoring interstory drift in buildings under seismic loading using MEMS inclinometers. Construct. Build. Mater. 185, 453–467.
Jeong, J.H., Jo, H., 2022. Real-time generic target tracking for structural displacement monitoring under environmental uncertainties via deep learning. Struct. Control Health Monit. 29 (3), e2902.
Jiao, J., Guo, J., Fujita, K., Takewaki, I., 2021. Displacement measurement and nonlinear structural system identification: a vision-based approach with camera motion correction using planar structures. Struct. Control Health Monit. 28 (8), e2761.
Kaplan, E., Hegarty, C.J., 2017. Understanding GPS/GNSS: Principles and Applications, third ed. Artech House, Boston ; London.
Khuc, T., Catbas, F.N., 2017a. Computer vision-based displacement and vibration monitoring without using physical target on structures. Struct. Infrastruct. Eng. 13 (4), 505–516.
Khuc, T., Catbas, F.N., 2017b. Completely contactless structural health monitoring of real-life structures using cameras and computer vision. Struct. Control Health Monit. 24 (1), e1852.
Kim, N.S., Cho, N.S., 2004. Estimating deflection of a simple beam model using fiber optic bragg-grating sensors. Exp. Mech. 44 (4), 433–439.
Kim, K., Sohn, H., 2017. Dynamic displacement estimation by fusing LDV and LiDAR measurements via smoothing based Kalman filtering. Mech. Syst. Signal Process. 82, 339–355.
Kim, K., Sohn, H., 2020. Dynamic displacement estimation for long-span bridges using acceleration and heuristically enhanced displacement measurements of real-time kinematic global navigation system. Sensors 20 (18), 5092.
Kim, J., Kim, K., Sohn, H., 2013. In situ measurement of structural mass, stiffness, and damping using a reaction force actuator and a laser Doppler vibrometer. Smart Mater. Struct. 22 (8), 085004.
Kim, J., Kim, K., Sohn, H., 2014. Autonomous dynamic displacement estimation from data fusion of acceleration and intermittent displacement measurements. Mech. Syst. Signal Process. 42 (1), 194–205.

Kim, K., Kim, J., Sohn, H., 2016a. Development and full-scale dynamic test of a combined system of heterogeneous laser sensors for structural displacement measurement. Smart Mater. Struct. 25 (6), 065015.
Kim, K., Jaemook, C., Koo, G., Sohn, H., 2016b. Dynamic displacement estimation by fusing biased high-sampling rate acceleration and low-sampling rate displacement measurements using two-stage Kalman estimator. Smart Struct. Syst. 17, 647–667.
Kim, K., Choi, J., Chung, J., Koo, G., Bae, I.H., Sohn, H., 2018. Structural displacement estimation through multi-rate fusion of accelerometer and RTK-GPS displacement and velocity measurements. Measurement 130, 223–235.
Koo, G., Kim, K., Chung, J.Y., Choi, J., Kwon, N.Y., Kang, D.Y., et al., 2017. Development of a high precision displacement measurement system by fusing a low cost RTK-GPS sensor and a force feedback accelerometer for infrastructure monitoring. Sensors 17 (12), 2745.
Lee, J., Kim, R.E., 2022. Noncontact dynamic displacements measurements for structural identification using a multi-channel Lidar. Struct. Control Health Monit. 29 (11), e3100.
Lee, J.J., Shinozuka, M., 2006. A vision-based system for remote sensing of bridge displacement. NDT E Int. 39 (5), 425–431.
Lee, J.J., Cho, S., Shinozuka, M., Yun, C.B., Lee, C.G., Lee, W.T., 2006. Evaluation of bridge load carrying capacity based on dynamic displacement measurement using real-time image processing techniques. Int. J. Steel Struct. 6, 377–385.
Lee, H.S., Hong, Y.H., Park, H.W., 2010. Design of an FIR filter for the displacement reconstruction using measured acceleration in low-frequency dominant structures. Int. J. Numer. Methods Eng. 82 (4), 403–434.
Lee, J., Lee, K.C., Lee, S., Lee, Y.J., Sim, S.H., 2019. Long-term displacement measurement of bridges using a LiDAR system. Struct. Control Health Monit. 26 (10), e2428.
Lee, J., Lee, K.C., Jeong, S., Lee, Y.J., Sim, S.H., 2020. Long-term displacement measurement of full-scale bridges using camera ego-motion compensation. Mech. Syst. Signal Process. 140.
Lee, Z.K., Bonopera, M., Hsu, C.C., Lee, B.H., Yeh, F.Y., 2022a. Long-term deflection monitoring of a box girder bridge with an optical-fiber, liquid-level system. Structures 44, 904–919.
Lee, S., Kim, H., Sim, S.H., 2022b. Nontarget-based displacement measurement using LiDAR and camera. Autom. ConStruct. 142, 104493.
Lee, J., Jeong, S., Kim, H., Lee, K.C., Sim, S.H., 2022c. Comparative study of long-term displacement measurement methods – Focusing on a Pre-stressed concrete bridge under construction. Measurement 201, 111691.
Liu, Y., Deng, Y., Cai, C.S., 2015. Deflection monitoring and assessment for a suspension bridge using a connected pipe system: a case study in China. Struct. Control Health Monit. 22 (12), 1408–1425.
Luan, L., Zheng, J., Wang, M.L., Yang, Y., Rizzo, P., Sun, H., 2021. Extracting full-field subpixel structural displacements from videos via deep learning. J. Sound Vib. 505, 116142.
Luo, L., Feng, M.Q., 2018. Edge-enhanced matching for gradient-based computer vision displacement measurement. Comput. Aided Civ. Infrastruct. Eng. 33 (12), 1019–1040.
Luo, L., Feng, M.Q., Wu, J., 2020. A comprehensive alleviation technique for optical-turbulence-induced errors in vision-based displacement measurement. Struct. Control Health Monit. 27 (3), e2496.
Lydon, D., Lydon, M., del Rincón, J.M., Taylor, S.E., Robinson, D., O'Brien, E., et al., 2018. Development and field testing of a time-synchronized system for multi-point displacement calculation using low-cost wireless vision-based sensors. IEEE Sensor. J. 18 (23), 9744–9754.
Lynch, J.P., 2007. An overview of wireless structural health monitoring for civil structures. Phil. Trans. Math. Phys. Eng. Sci. 365 (1851), 345–372.
Ma, Z., Sohn, H., 2019. Structural displacement estimation by FIR filter based fusion of strain and acceleration measurements. In: The 29th International Ocean and Polar Engineering Conference. OnePetro.
Ma, Z., Chung, J., Liu, P., Sohn, H., 2021. Bridge displacement estimation by fusing accelerometer and strain gauge measurements. Struct. Control Health Monit. 28 (8), e2733.
Ma, Z., Choi, J., Sohn, H., 2022a. Noncontact cable tension force estimation using an integrated vision and inertial measurement system. Measurement 199, 111532.
Ma, Z., Choi, J., Sohn, H., 2022b. Real-time structural displacement estimation by fusing asynchronous acceleration and computer vision measurements. Comput. Aided Civ. Infrastruct. Eng. 37 (6), 688–703.
Ma, Z., Choi, J., Liu, P., Sohn, H., 2022c. Structural displacement estimation by fusing vision camera and accelerometer using hybrid computer vision algorithm and adaptive multi-rate Kalman filter. Autom. ConStruct. 140, 104338.
Ma, Z., Choi, J., Sohn, H., 2022d. Structural Displacement Estimation through the Fusion of FMCW Millimeter Wave Radar and Accelerometer. The 8th World Conference on Structural Control and Monitoring.
Ma, Z., Choi, J., Sohn, H., 2022e. Simultaneous displacement and cable force estimation for submerged floating tunnel based on strain and acceleration measurements. In: Bridge Safety, Maintenance, Management, Life-Cycle, Resilience and Sustainability. CRC Press.
Ma, Z., Choi, J., Yang, L., Sohn, H., 2023a. Structural displacement estimation using accelerometer and FMCW millimeter wave radar. Mech. Syst. Signal Process. 182, 109582.
Ma, Z., Choi, J., Jang, J., Kwon, O., Sohn, H., 2023b. Simultaneous estimation of submerged floating tunnel displacement and mooring cable tension through FIR filter based strain and acceleration fusion. Struct. Control Health Monit. 2023, e7803876.
MLTM. Korea, 2010. Highway Bridge Design Code (In Korean). Ministry of Land, Infrastructure and Transport, Seoul.
Mohurd, G.B., 2020. 50017–2017 Code for Design of Steel Structures (In Chinese). China Machine Press, Beijing.
Monserrat, O., Crosetto, M., Luzi, G., 2014. A review of ground-based SAR interferometry for deformation measurement. ISPRS J. Photogrammetry Remote Sens. 93, 40–48.
Moreu, F., Li, J., Jo, H., Kim, R.E., Scola, S., Spencer, B.F., et al., 2016. Reference-Free displacements for condition assessment of timber railroad bridges. J. Bridge Eng. 21 (2), 04015052.
Moschas, F., Stiros, S., 2011. Measurement of the dynamic displacements and of the modal frequencies of a short-span pedestrian bridge using GPS and an accelerometer. Eng. Struct. 33 (1), 10–17.
Mot. Jt/T, 2022. 1037–2022 Technical Specifications of Structural Monitoring for Highway Bridges (In Chinese). China Communications Press, Beijing.
Nakamura, S ichi, 2000. GPS measurement of wind-induced suspension bridge girder displacements. J. Struct. Eng. 126 (12), 1413–1419.
Nasimi, R., Moreu, F., 2021a. A methodology for measuring the total displacements of structures using a laser–camera system. Comput. Aided Civ. Infrastruct. Eng. 36 (4), 421–437.
Nasimi, R., Moreu, F., 2021b. Development and implementation of a laser–camera–UAV system to measure total dynamic transverse displacement. J. Eng. Mech. 147 (8), 04021045.
Nassif, H.H., Gindy, M., Davis, J., 2005. Comparison of laser Doppler vibrometer with contact sensors for monitoring bridge deflection and vibration. NDT E Int. 38 (3), 213–218.
Niu, Y., Ye, Y., Zhao, W., Shu, J., 2021. Dynamic monitoring and data analysis of a long-span arch bridge based on high-rate GNSS-RTK measurement combining CF-CEEMD method. J. Civ. Struct. Health Monit. 11 (1), 35–48.
Owerko, T., Kuras, P., 2019. Effective Processing of Radar Data for Bridge Damage Detection. Shock Vib. CT, e2621092.
Ozdagli, A.I., Gomez, J.A., Moreu, F., 2017. Real-time reference-free displacement of railroad bridges during train-crossing events. J. Bridge Eng. 22 (10), 04017073.
Ozdagli, A.I., Liu, B., Moreu, F., 2018. Low-cost, efficient wireless intelligent sensors (LEWIS) measuring real-time reference-free dynamic displacements. Mech. Syst. Signal Process. 107, 343–356.
Park, H.S., Lee, H.M., Adeli, H., Lee, I., 2007. A new approach for health monitoring of structures: terrestrial laser scanning. Comput. Aided Civ. Infrastruct. Eng. 22 (1), 19–30.
Park, J.W., Sim, S.H., Jung Jr., H.J., 2013a. BFS. Development of a wireless displacement measurement system using acceleration responses. Sensors 13 (7), 8377–8392.
Park, J.W., Sim, S.H., Jung, H.J., 2013b. Displacement estimation using multimetric data fusion. IEEE ASME Trans. Mechatron. 18 (6), 1675–1682.
Park, J.W., Sim, S.H., Jung, H.J., 2014. Wireless displacement sensing system for bridges using multi-sensor fusion. Smart Mater. Struct. 23 (4), 045022.
Park, J.W., Moon, D.S., Yoon, H., Gomez, F., Spencer Jr., B.F., Kim, J.R., 2018. Visual–inertial displacement sensing using data fusion of vision-based displacement with acceleration. Struct. Control Health Monit. 25 (3), e2122.
Pehlivan, H., 2022. Identification of structural displacements utilizing concurrent robotic total station and GNSS measurements. Smart Struct. Syst. 30 (4), 411–420.
Psimoulis, P.A., Stiros, S.C., 2007. Measurement of deflections and of oscillation frequencies of engineering structures using Robotic Theodolites (RTS). Eng. Struct. 29 (12), 3312–3324.
Ramakrishnan, M., Rajan, G., Semenova, Y., Farrell, G., 2016. Overview of fiber optic sensor technologies for strain/temperature sensing applications in composite materials. Sensors 16 (1), 99.
Reu, P.L., Rohe, D.P., Jacobs, L.D., 2017. Comparison of DIC and LDV for practical vibration and modal measurements. Mech. Syst. Signal Process. 86, 2–16.
Rodrigues, C., Félix, C., Figueiras, J., 2011. Fiber-optic-based displacement transducer to measure bridge deflections. Struct. Health Monit. 10 (2), 147–156.
Rodrigues, D.V.Q., Zuo, D., Li, C., 2021. Wind-induced displacement analysis for a traffic light structure based on a low-cost Doppler radar array. IEEE Trans. Instrum. Meas. 70, 1–9.
Santhosh, K.V., Roy, B.K., 2012. A smart displacement measuring technique using linear variable displacement transducer. Procedia Technol. 4, 854–861.
Santhosh, K.V., Roy, B.K., 2017. Online implementation of an adaptive calibration technique for displacement measurement using LVDT. Appl. Soft Comput. 53, 19–26.
Shajihan, S.A.V., Hoang, T., Mechitov, K., Spencer Jr., B.F., 2022. Wireless SmartVision system for synchronized displacement monitoring of railroad bridges. Comput. Aided Civ. Infrastruct. Eng. 37 (9), 1070–1088.
Shang, Z., Shen, Z., 2018. Multi-point vibration measurement and mode magnification of civil structures using video-based motion processing. Autom. ConStruct. 93, 231–240.
Shao, Y., Li, L., Li, J., An, S., Hao, H., 2021. Computer vision based target-free 3D vibration displacement measurement of structures. Eng. Struct. 246, 113040.
Shao, Y., Li, L., Li, J., An, S., Hao, H., 2022. Target-free 3D tiny structural vibration measurement based on deep learning and motion magnification. J. Sound Vib. 538, 117244.
Shen, S., Wu, Z., Yang, C., Wan, C., Tang, Y., Wu, G., 2010. An improved conjugated beam method for deformation monitoring with a distributed sensitive fiber optic sensor. Struct. Health Monit. 9 (4), 361–378.
Shen, N., Chen, L., Liu, J., Wang, L., Tao, T., Wu, D., et al., 2019. A review of global navigation satellite system (GNSS)-Based dynamic monitoring technologies for structural health monitoring. Rem. Sens. 11 (9), 1001.
Shin, S., Lee, S.U., Kim, Y., Kim, N.S., 2012. Estimation of bridge displacement responses using FBG sensors and theoretical mode shapes. Struct. Eng. Mech. 42 (2), 229–245.
Sigurdardottir, D.H., Stearns, J., Glisic, B., 2017. Error in the determination of the deformed shape of prismatic beams using the double integration of curvature. Smart Mater. Struct. 26 (7), 075002.
Spencer, B.F., Hoskere, V., Narazaki, Y., 2019. Advances in computer vision-based civil infrastructure inspection and monitoring. Eng. 5 (2), 199–222.

Stiros, S.C., Psimoulis, P.A., 2012. Response of a historical short-span railway bridge to passing trains: 3-D deflections and dominant frequencies derived from Robotic Total Station (RTS) measurements. Eng. Struct. 45, 362–371.
Sun, L., Li, Y., Zhang, W., 2020. Experimental study on continuous bridge-deflection estimation through inclination and strain. J. Bridge Eng. 25 (5), 04020020.
Sun, Z., Siringoringo, D.M., Fujino, Y., 2021. Load-carrying capacity evaluation of girder bridge using moving vehicle. Eng. Struct. 229, 111645.
Tamura, Y., Matsui, M., Pagnini, L.C., Ishibashi, R., Yoshida, A., 2002. Measurement of wind-induced response of buildings using RTK-GPS. J. Wind Eng. Ind. Aerod. 90 (12), 1783–1793.
Toyoshima, M., Ohashi, T., Shinohara, S., Yoshida, H., Ikeda, H., Sumi, M., 1994. New digital displacement measuring circuit for aperiodic vibration using self-mixing type LDV. In: Conference Proceedings. 10th Anniversary. IMTC/94. Advanced Technologies in I & M. 1994 IEEE Instrumentation and Measurement Technolgy Conference. IEEE *(Cat. No. 94CH3424-9)*.
Vanicek, P., Castle, R.O., Balazs, E.I., 1980. Geodetic leveling and its applications. Rev. Geophys. 18 (2), 505–524.
Vicente, M.A., González, D.C., Fu, G., 2015. Static and dynamic testing of high-speed rail bridges in Spain. J. Bridge Eng. 20 (2), 06014006.
Wang, R., Schurr, B., Milkereit, C., Shao, Z., Jin, M., 2011. An improved automatic scheme for empirical baseline correction of digital strong-motion records. Bull. Seismol. Soc. Am. 101 (5), 2029–2044.
Wang, Z.C., Geng, D., Ren, W.X., Liu, H.T., 2014. Strain modes based dynamic displacement estimation of beam structures with strain sensors. Smart Mater. Struct. 23 (12), 125045.
Wang, X., Zhao, Q., Xi, R., Li, C., Li, G., Li, L., 2021. Review of bridge structural health monitoring based on GNSS: from displacement monitoring to dynamic characteristic identification. IEEE Access 9, 80043–80065.
Weng, Y., Shan, J., Lu, Z., Lu, X., Spencer Jr., B.F., 2021. Homography-based structural displacement measurement for large structures using unmanned aerial vehicles. Comput. Aided Civ. Infrastruct. Eng. 36 (9), 1114–1128.
Wu, R.T., Jahanshahi, M.R., 2020. Data fusion approaches for structural health monitoring and system identification: past, present, and future. Struct. Health Monit. 19 (2), 552–586.
Wu, Z., Liu, W., He, M., Jiang, D., 2022. Coupling displacement sensors with energy harvesting: a study of wireless self-powered displacement detection methods. Energy Rep. 8, 1471–1482.
Xi, R., Liang, Y., Chen, Q., Jiang, W., Chen, Y., Liu, S., 2022. Analysis of annual deformation characteristics of Xilongchi dam using historical GPS observations. Rem. Sens. 14 (16), 4018.
Xia, Y., Zhang, P., Ni, Y qing, Zhu, H ping, 2014. Deformation monitoring of a super-tall structure using real-time strain data. Eng. Struct. 67, 29–38.
Xiong, C., Wang, M., Chen, W., 2022. Data analysis and dynamic characteristic investigation of large-scale civil structures monitored by RTK-GNSS based on a hybrid filtering algorithm. J. Civ. Struct. Health Monit. 12 (4), 857–874.
Xu, Y., Brownjohn, J.M.W., 2018. Review of machine-vision based methodologies for displacement measurement in civil structures. J. Civ. Struct. Health Monit. 8 (1), 91–110.
Xu, Y., Brownjohn, J.M.W., Hester, D., Koo, K.Y., 2017. Long-span bridges: enhanced data fusion of GPS displacement and deck accelerations. Eng. Struct. 147, 639–651.
Xu, Y., Brownjohn, J.M., Huseynov, F., 2019. Accurate deformation monitoring on bridge structures using a cost-effective sensing system combined with a camera and accelerometers: case study. J. Bridge Eng. 24 (1), 05018014.
Xu, Y., Zhang, J., Brownjohn, J., 2021. An accurate and distraction-free vision-based structural displacement measurement method integrating Siamese network based tracker and correlation-based template matching. Measurement 179, 109506.
Yang, D., Zhang, S., Wang, S., Yu, Q., Su, Z., Zhang, D., 2022. Real-time Illumination Adjustment for Video Deflectometers. Struct. Control Health Monit. 29 (5), e2930.
Ye, X.W., Ni, Y.Q., Wai, T.T., Wong, K.Y., Zhang, X.M., Xu, F., 2013. A vision-based system for dynamic displacement measurement of long-span bridges: algorithm and verification. Smart Struct. Syst. 12 (3), 363–379.
Yoon, H., Shin, J., Spencer Jr., B.F., 2018. Structural displacement measurement using an unmanned aerial system. Comput. Aided Civ. Infrastruct. Eng. 33 (3), 183–192.
Yu, S., Zhang, J., 2020. Fast bridge deflection monitoring through an improved feature tracing algorithm. Comput. Aided Civ. Infrastruct. Eng. 35 (3), 292–302.
Yu, J., Zhu, P., Xu, B., Meng, X., 2017. Experimental assessment of high sampling-rate robotic total station for monitoring bridge dynamic responses. Measurement 104, 60–69.
Yu, J., Meng, X., Yan, B., Xu, B., Fan, Q., Xie, Y., 2020. Global Navigation Satellite System-based positioning technology for structural health monitoring: a review. Struct. Control Health Monit. 27 (1), e2467.
Yu, Q., Yin, Y., Zhang, Y., Chen, W., Hu, B., Liu, X., 2022. Displacement measurement of large structures using nonoverlapping field of view multi-camera systems under six degrees of freedom ego-motion. Comput. Aided Civ. Infrastruct. Eng.
Zhang, W., Sun, L.M., Sun, S.W., 2017a. Bridge-Deflection estimation through inclinometer data considering structural damages. J. Bridge Eng. 22 (2), 04016117.
Zhang, J., Tian, Y., Yang, C., Wu, B., Wu, Z., Wu, G., et al., 2017b. Vibration and deformation monitoring of a long-span rigid-frame bridge with distributed long-gauge sensors. J. Aero. Eng. 30 (2), B4016014.
Zhang, Q., Zhang, J., Duan, W., Wu, Z., 2018a. Deflection distribution estimation of tied-arch bridges using long-gauge strain measurements. Struct. Control Health Monit. 25 (3), e2119.
Zhang, B., Ding, X., Werner, C., Tan, K., Zhang, B., Jiang, M., et al., 2018b. Dynamic displacement monitoring of long-span bridges with a microwave radar interferometer. ISPRS J. Photogrammetry Remote Sens. 138, 252–264.
Zhang, G., Wu, Y., Zhao, W., Zhang, J., 2020. Radar-based multipoint displacement measurements of a 1200-m-long suspension bridge. ISPRS J. Photogrammetry Remote Sens. 167, 71–84.
Zhang, Q., Fu, X., Ren, L., 2021. Deflection estimation of beam structures based on the measured strain mode shape. Smart Mater. Struct. 30 (10), 105003.
Zhang, Q., Fu, X., Ren, L., Li, H.N., 2023. Two-dimensional full-field displacement reconstruction of lattice towers using data fusion method: theoretical study and experimental validation. Thin-Walled Struct. 182, 110189.
Zhou, J., Xiao, H., Jiang, W., Bai, W., Liu, G., 2020a. Automatic subway tunnel displacement monitoring using robotic total station. Measurement 151, 107251.
Zhou, H.F., Lu, L.J., Li, Z.Y., Ni, Y.Q., 2020b. Exploration of temperature effect on videogrammetric technique for displacement monitoring. Smart Struct. Syst. 25 (2), 135–153.
Zhou, J., Sun, Z., Wei, B., Zhang, L., Zeng, P., 2021. Deflection-based multilevel structural condition assessment of long-span prestressed concrete girder bridges using a connected pipe system. Measurement 169, 108352.
Zhou, Q., Li, Q.S., Han, X.L., Wan, J.W., Xu, K., 2022. Horizontal displacement estimation of high-rise structures by fusing strain and acceleration measurements. J. Build. Eng. 57, 104964.
Zhu, H., Gao, K., Xia, Y., Gao, F., Weng, S., Sun, Y., et al., 2020. Multi-rate data fusion for dynamic displacement measurement of beam-like supertall structures using acceleration and strain sensors. Struct. Health Monit.- An Int. J. 19 (2), 520–536.
Zhu, J., Zhang, C., Lu, Z., Li, X., 2021. A multi-resolution deep feature framework for dynamic displacement measurement of bridges using vision-based tracking system. Measurement 183, 109847.
Zhuang, Y., Chen, W., Jin, T., Chen, B., Zhang, H., Zhang, W., 2022. A review of computer vision-based structural deformation monitoring in field environments. Sensors 22 (10), 3789.
Zhuojiang, N., Wei, T., Hui, Z., 2021. Development of a small-size laser triangulation displacement sensor and temperature drift compensation method. Meas. Sci. Technol. 32 (9), 095107.